Chapter 3

Experimental Method

The B mixing can be studied with two distinct methods. In a first method, only the total rate of events in which one B changes flavour between the time of production and that of decay is determined independently of the time at which the decay occurs. The particle-antiparticle oscillation is therefore integrated over time. In the second method, instead, the time dependence shown in Chapter 2, Section 2.2, is measured, and the actual oscillation frequency is extracted from that distribution. These methods are known as *time-integrated mixing* and *oscillation* measurements. Both methods were successfully used for B_d mesons studies [45, 46, 47, 48, 49]. While the slow oscillation frequency of B_d mesons allows information to be extracted from the time-integrated mixing measurements, the situation is different in the case of B_s mesons. As a consequence of their rapid oscillation frequency with respect to the decay time, half of the B_s mesons are found, when they decay, in a flavour different from that at production. The time-integrated measurement is therefore insensitive to the oscillation frequency.

To start this Chapter, the basic features of the time-integrated and oscillation measurement methods are given, and general techniques used in B-mixing analyses are explained. The main experimental issues are reviewed, with special emphasis on the factors which limit the sensitivity. The most important differences between the experimental studies on B_d and B_s oscillations are explained. The impact of the experimental resolution on the reconstructed B-meson proper time (*i.e.*, the B meson decay time in its rest frame, see Section 3.1.1) is discussed in detail, for instance. In the case of B_s mesons, contrary to B_d mesons, the proper time resolution is crucial. Although the experimental description is centred on relevant issues for data taken at the Z peak (at LEP and SLC), a brief description of the B-mixing measurements performed at CLEO or CDF is also given.

In the case of oscillation studies, a fit to the expected proper time distribution is performed. The fitting procedure is explained in Section 3.2. The fit for B_s oscillations is most often performed with the *amplitude method* [9, 56]. In this method, an amplitude $\mathcal{A}$ is introduced in front of the oscillating term in the probability density function for B_s mesons, (Eq. 2.20), and measured as a function of the oscillation frequency. The method is explained in detail in Section 3.3, along with a complete discussion of the expected dependence on the frequency of the measured amplitude and its uncertainty. The interpretation of the results in terms of the probability of being due to a statistical fluctuation is given.

3.1 Basic features of a B mixing measurement

Time-integrated measurement

The simplest experimental approach, and first used ever, for a measurement of the $B^0 - \overline{B}^0$ mixing consists in the estimation of the B^0 mesons fraction with a different flavour at the times of production and decay. If this fraction is zero, it means that there is no mixing in the system studied. If it is 50% it means that the oscillation is rapid enough to saturate the integrated method, rendering it insensitive to the actual oscillation frequency. Values in between can be turned into a measurement of the oscillation frequency (or equivalently, of the mass difference between the two mass eigenstates, Δm_{B_q}) as follows. The mixing parameter χ_q is defined as the average probability of a B_q^0 meson to be found in a $\overline{B}_q^0$ state at decay:

$$\chi_q = \frac{\int_0^\infty P_{B \to \overline{B}} dt}{\int_0^\infty P_{B \to B} dt + \int_0^\infty P_{B \to \overline{B}} dt} \; . \tag{3.1}$$

With the approximation of $\Delta\Gamma_q = 0$ and negligible CP violation in the mixing, as discussed in Section 2.2, χ_q reads

$$\chi_q \simeq \frac{(\Delta m_{B_q}/\Gamma_{B_q})^2}{2[1 + (\Delta m_{B_q}/\Gamma_{B_q})^2]} \; . \tag{3.2}$$

The time-integrated method has been successfully used for B_d mixing studies done with data taken at accelerators running at the energy of the $\Upsilon(4S)$ resonance [49]. This energy is just enough to allow the $\Upsilon(4S)$ to decay in a coherent $B_d^0 - \overline{B}_d^0$ or B^+-B^- pair, but it is too small for a $B_s^0 - \overline{B}_s^0$ pair to be produced. The first observation of B_d^0 mixing, by the ARGUS experiment, was obtained from the complete reconstruction of a single $B_d^0 - \overline{B}_d^0$ event in which the $\overline{B}_d^0$ had oscillated [43]: two B_d^0 were reconstructed, with the following decay chains: $B_d^0 \to D^{*-}\mu^+\nu_\mu$, with $D^{*-} \to \pi^-\overline{D^0}$, and $\overline{D^0} \to K^+\pi^-$, and the other, $B_d^0 \to D^{*-}\mu^+\nu_\mu$, with $D^{*-} \to \pi^0 D^-$, and $D^- \to K^+\pi^-\pi^-$. A display of this event is shown in Fig. 3.1. The presence of two B_d^0 in the final state is an unambiguous proof of the oscillation. However, complete reconstruction selections are very inefficient and therefore very few such fully-reconstructed events are available, and most of the sensitivity to χ_d for the experiments running at the $\Upsilon(4S)$ resonance, comes from events partially reconstructed. In most of the cases, two semileptonic decays are looked for, with like-sign leptons to identify events with a B_d^0 meson having oscillated.

Time-integrated mixing studies with similar techniques were performed in $p\overline{p}$ colliders (UA1 and CDF) [46] and at the Z resonance (SLD and LEP experiments) [47]. In both cases, however, B_d mesons are not the only contribution to mixing, B_s mesons also contribute to the integrated mixing rate. As a result, χ_d is not directly measurable, and the measured quantity $\overline{\chi}$ is an average of the B_d and B_s mesons integrated-mixing. The average mixing parameter is related to χ_d through,

$$\overline{\chi} = f_d \chi_d + f_s \chi_s \; , \tag{3.3}$$

where f_d and f_s are the fractions of $B_{d,s}$ in $b\overline{b}$ decays, and $\chi_s = 0.5$.

As already stated, B_s oscillations are too rapid to be studied in a time-integrated manner: only analyses which exploit the B-meson proper time information are sensitive to Δm_s.
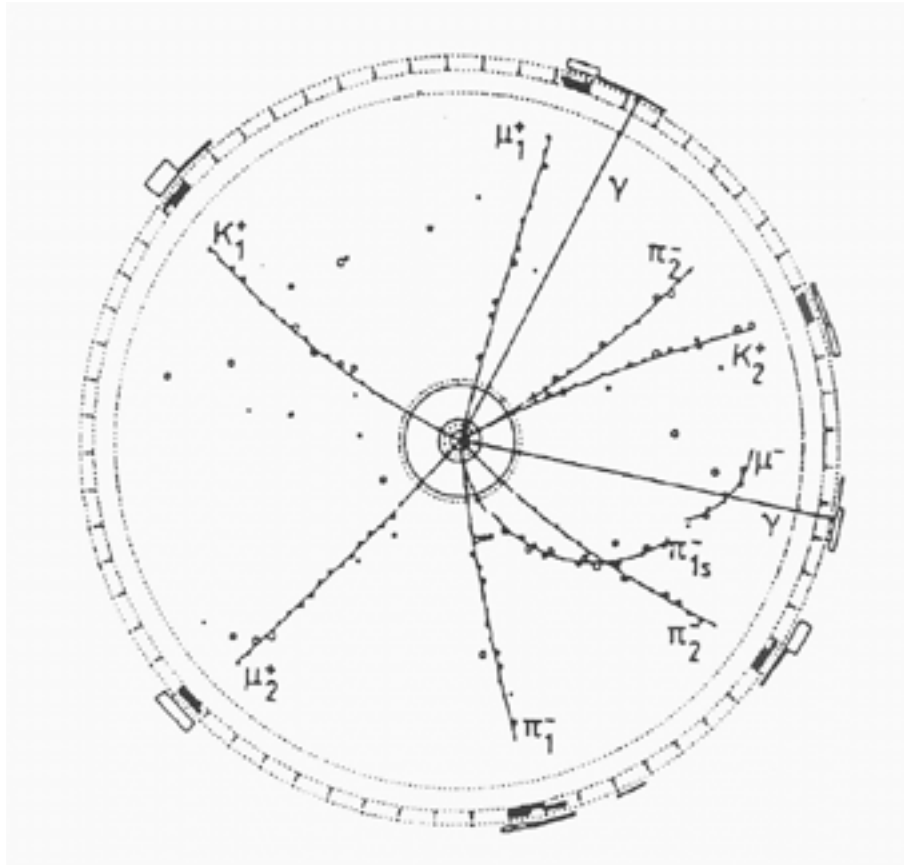
Figure 3.1: The golden event: first evidence for oscillations from the ARGUS Collaboration.

Oscillation measurement

Oscillation measurements aim at reconstructing the proper time distribution of B^0 meson decays shown in Eq. 2.2. To do so, more experimental information on the decay than in the case of time-integrated measurements is needed.

First, the proper time of the B^0 decay studied needs to be determined, although it is not a quantity directly measurable. Indeed it can only be inferred from two independent measurements: the decay length l, i.e. the distance of flight before decay, and the momentum p of the B^0 meson, both measured in the laboratory rest frame. These two measurements are described in Section 3.1.

It is also necessary to determine if the meson oscillated or not. To this end the b quark flavour (b or $\bar{b}$) of the B^0 meson has to be determined both at production (initial state) and decay (final state) identification. If they are identical the event is labelled as unmixed and as mixed otherwise. In general the analysis event selection is strongly determined by the technique used for the final state flavour determination. Details are given in Section 3.2.

The proper time and the mixed/unmixed label are the two main pieces of information needed for an oscillation measurement, and would actually be the only needed in a pure

sample of B_s (or B_d) mesons. However, such pure samples cannot be isolated at the Z-boson pole or at the p$\overline{\text{p}}$ colliders. Further selection must be performed to isolate as much as possible the kind of events desired. Some of the most common approaches for signal enrichment and background evaluation are given in Section 3.1.3.

Although oscillation studies are done for both B_d an B_s mesons systems, the oscillation frequency Δm_d and Δm_s are of different enough magnitude to render the experimental key issues in both cases quite different. To illustrate this point, the proper time distributions expected in both cases are presented in Fig. 3.2. In the case of B_d oscillations, the frequency,
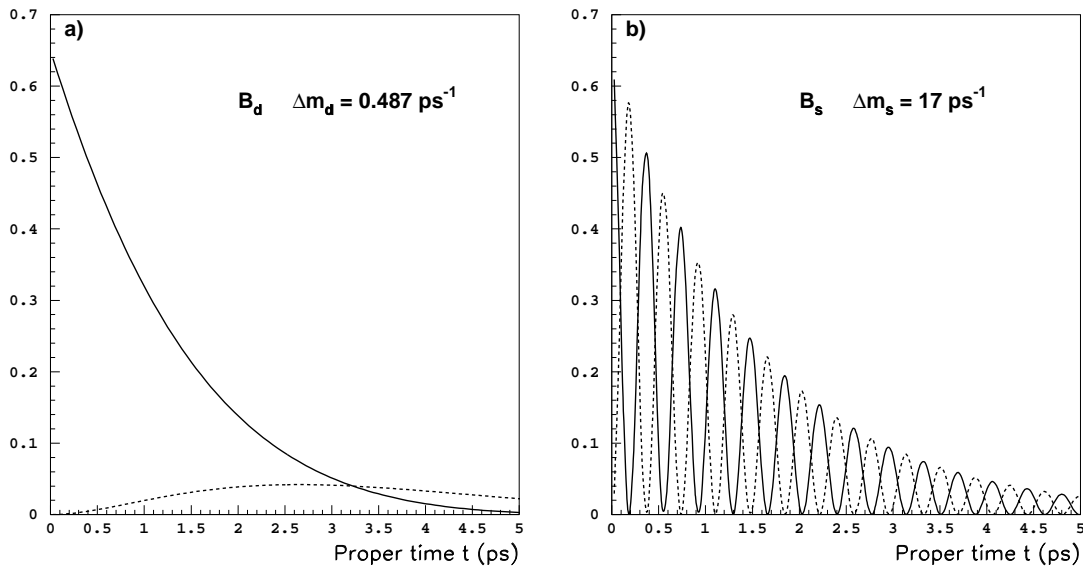

Figure 3.2: Proper time distribution for mixed/unmixed B_d and B_s mesons. Full curve holds for unmixed and dotted for mixed events.

already measured with good accuracy, is small. As it is shown Fig. 3.2a, the proper time distribution expected for mixed and unmixed events can be disentangled even with a moderate proper time resolution (typical values of the proper time resolution achieved at LEP are of the order of 0.3 ps, already excellent for that purpose). For B_s mesons, however, the rapid oscillation frequency (for illustration $\Delta m_s = 17\,\text{ps}^{-1}$ is taken) makes the analysis complicated and renders the proper time resolution crucial. The distributions shown in Fig. 3.2 refer to the expectations in the case of perfect mixed/unmixed labelling. When the experimental uncertainty on this labelling is taken into account, the difference between mixed and unmixed proper time distributions is diluted. A B_s oscillation frequency measurement, never achieved yet, requires excellent proper time resolution as well as very good performance in flavour tagging.

All the ingredients of such an oscillation analysis are described in detail in the following Sections. The experimental techniques described apply to B_s oscillations analyses, but in most of the cases they are similar to those used for B_d studies.

3.1.1 Proper time measurement

The determination of the B meson proper time, *i.e.*, the B meson lifetime as evaluated in its own rest frame, requires the measurement of its decay length and its momentum in the laboratory rest frame. The experimental technique often depends on the event selection. Some of the general aspects are given in this Section. More details, closely related to the main analysis described in this thesis, can be found in Chapter 6.

The decay length of the B meson is the three-dimensional distance between the point where the primary interaction takes place (*i.e.*, the e^+e^- annihilation, in the case of LEP), and the point where the flying meson decays. The main interaction point determination is not specific to a B oscillation analysis and depends on the experimental environment where the data are taken. The method used by the ALEPH experiment is explained in Section 5.4. The secondary vertex, *i.e.*, the point where the B meson decays, is determined with different methods depending on the event selection. The best resolutions are achieved for exclusive decay reconstructions. In this configuration all the secondary particles are identified and their common vertex position can be determined with high precision. For more inclusive selections, topological techniques lead to much worse resolutions. In some cases, for semileptonic decays for instance, the decay vertex is obtained from hybrid techniques, in which a fraction of the decay particles are identified.

The B meson momentum measurement depends on the event selection as well. If the decay is exclusively reconstructed, it is determined as the sum of the momenta of all decaying particles and the resolution is excellent by construction. The momentum of the jet in which the secondary vertex is found is taken as the meson momentum for an inclusive event selection. In the case of semileptonic decays, a fraction of the B meson momentum is carried by a neutrino which escapes the experiment without detection. The neutrino momentum is estimated from the requirement of energy and momentum conservation in the event (the quality of this technique depends strongly on the experimental environment where the data are taken, it is successfully used at the ALEPH experiment, as explained in Section 6.7.1). The B momentum is then estimated as the sum of the lepton and the charm candidate momenta, complemented with the neutrino momentum estimate.

Even though the exclusive reconstruction of decays has the advantage of an almost perfect resolution, it implies a very tight selection. The resulting data samples available are therefore statistically poor. In contrast, the event selection for an ultimate B oscillation measurement has to be a compromise between exclusiveness to obtain good resolution and inclusiveness to gain from statistics. The analysis described in Chapter 6 is based on an inclusive semileptonic selection, which constitutes the best compromise in the LEP environment. For the SLD experiment the situation is different. The data sample is ten times smaller than in a LEP experiment but the intrinsic resolution of the tracking is better by a factor of 3. That makes SLD data more adequate for analyses based on a fully inclusive selection. At the CDF experiment, being on a $p\overline{p}$ collider, inclusive or semi-inclusive techniques are not viable, only exclusive (or close to exclusive) methods are possible.

The proper time t is determined from the decay length l and the momentum p of the B meson as

$$t = \frac{l\,m}{p\,c}\;,\tag{3.4}$$

where m is the B meson mass, and c is the speed of light. The proper time resolution can be therefore expressed, by differentiation, as a function of the decay length and momentum resolutions as

$$\sigma_t \,=\, \frac{m}{p\,c}\,\sigma_l \,\oplus\, t\,\frac{\sigma_p}{p} \;, \tag{3.5}$$

where σ_l is the decay length resolution, and σ_p/p the relative momentum resolution. The second term of Eq. 3.5 is proportional to the measured proper time itself. In the case of B_s mesons, the period of the oscillation is much shorter than the lifetime, therefore the sensitivity comes mostly from short lived mesons, for which the contribution of the momentum resolution vanishes. The sensitivity of an inclusive analysis is then limited by the resolution on the decay length. In the case of B_d oscillations, a significant mixing rate is observed only at proper times larger than a lifetime ($t > \tau_{B_d}$). Therefore the momentum resolution term dominates the proper time reconstruction uncertainty, which is anyway not a crucial issue for those analyses.

3.1.2   Flavour tagging

The b-quark flavour of the B meson needs to be determined at production and decay and compared to each other to establish the unmixed/mixed label of each data event.

Three different techniques have been used to date for the final state (decay) flavour determination, depending on the event selection performed.

- In the case of exclusive reconstruction of flavour eigenstates there is no ambiguity. The decay chain establishes if the parent meson was a B^0 or a $\overline{B}^0$. Examples of exclusive reconstruction oscillation analyses are found in Refs. [57, 58] and in Section 7.2.

- For semileptonic decays, the electric charge of the lepton is used as a tag. Figure 3.3 shows the Feynman diagrams for semileptonic decays of both B^0 and $\overline{B}^0$. A lepton
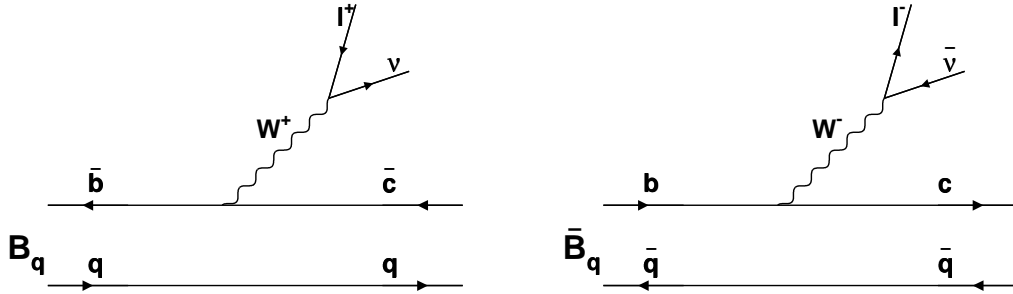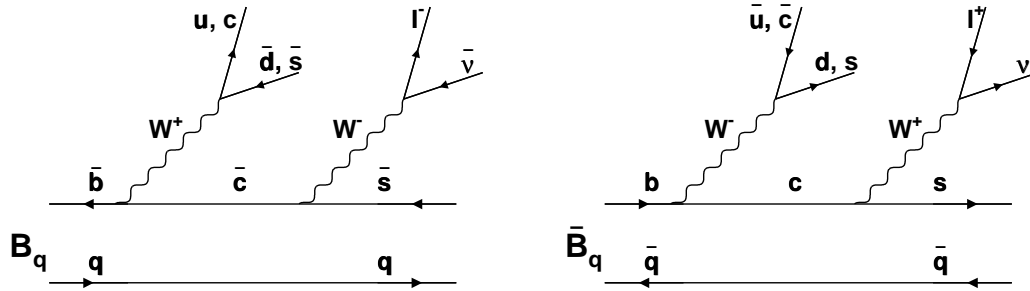

Figure 3.3: Semileptonic B^0 meson decay diagrams.

with negative electric charge originates from $\overline{B}^0$ and a positively charged lepton from a B^0. However, the presence of a lepton in the final state does not guarantee a direct semileptonic decay. Cascade decays with $b \rightarrow c \rightarrow \ell$ are also frequent, and have the opposite lepton-quark electric charge sign correlation (the corresponding diagrams are

Figure 3.4: Cascade B^0 meson decay diagrams.

shown in Fig. 3.4). These cascade decays need to be rejected from the final data sample. Additional cascades decays with b $\to \bar{\text{c}} \to \ell$ are also present (Fig. 3.5). The charge correlation between the lepton and the b quark is the same as in direct semileptonic decays, therefore no specific rejection for these decays is required. Examples of oscillation
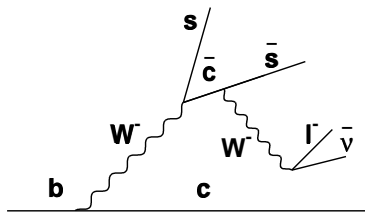
Figure 3.5: Cascade b $\to \bar{\text{c}} \to \ell$ decay diagram.

analyses using semileptonic selections are found in Refs.[58, 59].

- In the case of an inclusive selection, no decay particle is identified. A different method has to be used. An inclusive variable sensitive to the charge flow between the secondary and the tertiary vertices is used to statistically separate B^0 from $\overline{B}^0$ decays. In the case of SLD, their excellent tracking resolution is exploited which allows the tertiary vertex to be inclusively reconstructed. A dipole, $|Q_D - Q_B| \times |\vec{V}_D - \vec{V}_B|$, is formed and used as a final state tagging variable [60].

In e^+e^- and $p\bar{p}$ collisions, b-quarks are produced in $b\bar{b}$ pairs. Therefore, in addition to the B meson studied for mixing, the event contains another b-hadron with a b-flavour opposite to that of the B meson at production. The flavour of the B meson at production can therefore be determined from the flavour of the second b-hadron in the event. Some additional information is available from the fragmentation products of the B meson: the s-quark of the B_s meson (or d-quark for B_d) is created in a $s\bar{s}$ ($d\bar{d}$) pair, most of the times the second s-quark forms a kaon (pion) the electric charge of which (if non zero) is correlated with that of the B meson. The two pieces of information can be combined to obtain a single estimator of the initial b-flavour of the B meson. At SLC, the e^+e^- beams are polarized, which allows the b-forward-backward asymmetry to be used to further improve the initial

state b-flavour tagging. Typical effective values of the probability of incorrect initial state flavour assignment, the initial mistag, at LEP are around $\eta_I \sim 25\%$ while at SLD, mostly thanks to the polarized beams, $\eta_I \sim 15\%$ can be reached.

The final label mixed/unmixed obtained for a particular B meson decay has a certain probability of being incorrect, which is called the total mistag probability, η_T. This quantity is evaluated from a combination of the mistag for the initial, η_I, and final state, η_F, of the B meson as

$$1 \,-\, 2\eta_T \,=\, (1 \,-\, 2\eta_I)\,(1 \,-\, 2\eta_F) \;. \tag{3.6}$$

The combined mistag probability can be evaluated on average in the selected sample, or, as it is done in most of the cases, computed event by event. Simulated events are usually used to convert the combined tagging variable of each event into a mistag probability. The use of event-by-event information increases significantly the statistical power of an oscillation analysis.

The mistag probability, η_T, is used in the fitting procedure to weight events according to their probability of being correctly tagged.

3.1.3   Signal enrichment and background evaluation

Inclusive or semi-inclusive event sample selections result on poor signal purity: as in an unbiased $b\bar{b}$ sample, only about 10% of the events contain B_s meson decays. Some decay properties like the estimated electric charge of the secondary vertex, or the presence of kaons both in the fragmentation and the decay of the B_s candidate, can be used to statistically increase the effective signal purity. All the relevant discriminant variables are combined, and the result is used to define an event-by-event signal purity. More detailed explanations on this subject are given in Section 6.9.

Semi-exclusive selections, like the $D_s\ell$ reconstruction explained in Section 7.1, have an average signal purity of the order of 40%. The effective signal purity can still be increased with techniques similar to those used in inclusive selections. In the case of hadronic reconstruction of specific decays, the average purity is even higher, of the order of 60%, and can be increased in an analogous manner with the B_s constructed mass as a key discriminant variable.

The non-signal components in the selected sample, the background, need to be identified and properly characterized. In the case of inclusive or semi-inclusive selections, the background contains mostly other b-hadrons (B_d, $B^{+/-}$, and b-baryons), but also a small fraction of hadrons formed with lighter quarks, called udsc-background in the following. The estimation of the relative amount of the background components is explained in Section 6.9, for the b-hadron species, and in Section 6.4, for the udsc background, in the case of the inclusive semileptonic selection. The background treatment of semi-exclusive or exclusive selections is slightly different and explained in Sections 7.1, 7.2.

3.1.4   Effect of mistag, background, and resolution

The non-perfect flavour tagging, the presence of background, and the finite detector resolution introduce a dilution on the oscillation signal studied. Figure 3.6 is used to illustrate

this point. On the three plots the expected fraction of events tagged as mixed is plotted
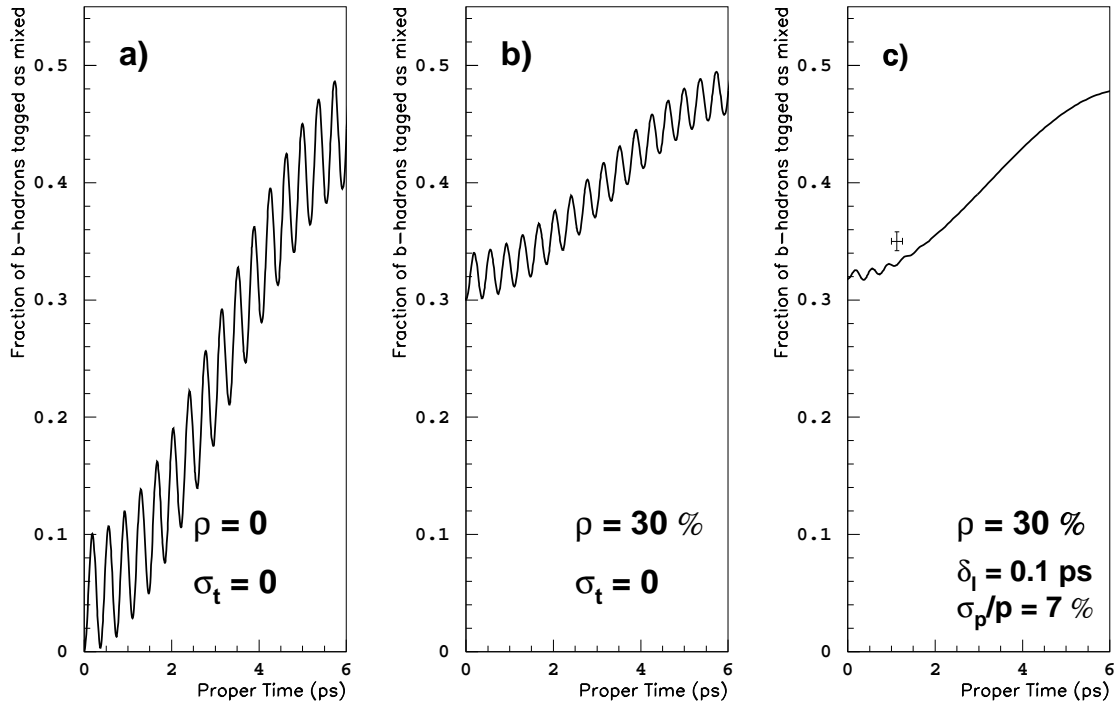

Figure 3.6: B_s oscillations signal resolution as a function of analysis parameters. The typical error bar for proper time values below 2 ps in an inclusive semileptonic analysis in ALEPH is shown.

as a function of the measured proper time. An inclusive selection with 10% B_s, 40% B_d, 40% B^+ and 10% b-baryons is considered, with oscillation frequencies $\Delta m_d = 0.487\,\mathrm{ps}^{-1}$ and $\Delta m_s = 17\,\mathrm{ps}^{-1}$. In Fig. 3.6a) perfect flavour tagging, both at production and decay, is assumed, as well as negligible proper time resolution. The rapid B_s meson oscillation is seen convoluted with the B_d mesons oscillation. In Fig. 3.6b) the effect of a global mistag probability of 30% is shown. The effective B_s oscillation amplitude is reduced rendering it more difficult to resolve. In Fig. 3.6c) the effect of the experimental resolution on the proper time measurement is also introduced, with momentum resolution $\sigma_p/p = 7\%$ and decay length resolution $\delta_l \equiv \sigma_l\, m/p_0\, c = 0.1\,\mathrm{ps}$ (these values are better than the average in most of the inclusive B_s oscillation analyses). As a consequence, B_s oscillations become only a marginal distortion on the B_d oscillation pattern, only visible at small proper time values. The typical experimental uncertainty for proper time values below 2 ps is shown both for the proper time and the asymmetry measurements in the case of an inclusive semileptonic analysis with the ALEPH data (Chapter 6). This last plot, compared to the others, is a clear illustration of the importance of the proper time resolution on B_s oscillations, as well as of the experimental difficulty of the measurement. The proper time resolution expression in Eq. 3.5 shows that the momentum resolution does not contribute at very small proper time values, the crucial issue for B_s oscillations analyses is therefore the decay length resolution.

3.2   Fitting procedure

Once the proper time of the selected B mesons and the mixed/unmixed label are determined, a fit to the expected proper time distribution is performed, to tentatively determine the value of the oscillation frequency.

A selected data sample is a mixture of signal, B_s mesons in this case, and different type of backgrounds. The probability density function ($p.d.f.$) has therefore to take into account the expected proper time properties of all the components in the sample, i) the oscillating signal component (B_s mesons); ii) the oscillating background component (B_d mesons); iii) the non-oscillation background component ($B^{+/-}$ and b-baryons); and iv) the udsc-background. The different parts of the $p.d.f.$ are explicited below for events labelled as unmixed and mixed.

- Oscillating B mesons (B_s and B_d mesons):

$$
\begin{aligned}
p.d.f.^{\mathrm{unmix}}(t) \;=\; f_{\mathrm{B_q}} \quad &\left[(1 - \eta_T) \, \frac{1 + \cos \Delta m_{\mathrm{Bq}} \, t_0}{2 \, \tau_{\mathrm{Bq}}} \; e^{-t_0/\tau_{\mathrm{Bq}}} \quad + \right. \\
&\left. \quad \eta_T \, \frac{1 - \cos \Delta m_{\mathrm{Bq}} \, t_0}{2 \, \tau_{\mathrm{Bq}}} \, e^{-t_0/\tau_{\mathrm{Bq}}} \right] \quad \otimes \quad \mathcal{R}(t_0, t) \,, \\
p.d.f.^{\mathrm{mix}}(t) \;=\; f_{\mathrm{B_q}} \quad &\left[(1 - \eta_T) \, \frac{1 - \cos \Delta m_{\mathrm{Bq}} \, t_0}{2 \, \tau_{\mathrm{Bq}}} \; e^{-t_0/\tau_{\mathrm{Bq}}} \quad + \right. \\
&\left. \quad \eta_T \, \frac{1 + \cos \Delta m_{\mathrm{Bq}} \, t_0}{2 \, \tau_{\mathrm{Bq}}} \, e^{-t_0/\tau_{\mathrm{Bq}}} \right] \quad \otimes \quad \mathcal{R}(t_0, t) \,.
\end{aligned}
\tag{3.7}
$$

- Non oscillating B hadrons ($B^{+/-}$ and b-baryons):

$$
\begin{aligned}
p.d.f.^{\mathrm{unmix}}(t) \;&=\; f_{\mathrm{B}} \left[(1 - \eta_T) \, \frac{e^{-t_0/\tau_{\mathrm{B}}}}{\tau_{\mathrm{B_d}}} \right] \quad \otimes \quad \mathcal{R}(t_0, t) \,, \\
p.d.f.^{\mathrm{mix}}(t) \;&=\; \quad f_{\mathrm{B}} \left[\eta_T \, \frac{e^{-t_0/\tau_{\mathrm{B}}}}{\tau_{\mathrm{B}}} \right] \quad \otimes \quad \mathcal{R}(t_0, t) \,.
\end{aligned}
\tag{3.8}
$$

- The udsc background is most often parametrized from simulated events.

$$
\begin{aligned}
p.d.f.^{\mathrm{unmix}}(t) \;&=\; f_{\mathrm{udsc}} \left[(1 - \eta_T) \, F^{\mathrm{simul}}(t) \right] \,, \\
p.d.f.^{\mathrm{mix}}(t) \;&=\; \quad f_{\mathrm{udsc}} \left[\eta_T \, F^{\mathrm{simul}}(t) \right] \,.
\end{aligned}
\tag{3.9}
$$

In the above expressions f_i ($i = B_q, B, \mathrm{udsc}$) are the fractions of each component in the selected sample, with $\sum_i f_i = 1$, and η_T is the mistag probability, which can be different for each component. The function $\mathcal{R}(t_0, t)$ is the proper time resolution function, built as a convolution of the decay length and momentum resolutions. All lifetimes, τ_i, are experimentally known, Δm_d is measured as well. The only free parameter, to be fit to the data, is the B_s oscillation frequency Δm_s.

The above expressions are used, convoluted with the experimental proper time efficiency, and resolution in a global likelihood function of the data sample minimized with respect to Δm_s. To date, no minimum deep enough for a Δm_s measurement has ever been found. Only lower limits on Δm_s have been set.

3.3 The amplitude method

Many different B_s oscillations analyses are being (or have been) performed by the LEP Collaborations, SLD and CDF. A method to easily combine their results and therefore increase the global final reach on Δm_s, known as the *amplitude method*, was first used by the ALEPH Collaboration [61] and is presented in Refs. [56, 9]. In this Section the basics of the method are explained, along with its interpretation.

The B_d oscillations are slow enough to allow the oscillation frequency Δm_d to be determined by several analyses in all experiments where b-hadrons are produced. An average value of Δm_d is obtained from the individual results of these analyses. In the case of B_s mesons, instead, as no analysis has yet been able to resolve the oscillation, the analogous approach is not applicable.

In the amplitude method the probability density function for the B_s signal is transformed by the introduction of the amplitude, $\mathcal{A}$, in front of the oscillation term as

$$p.d.f.^{\mathrm{u,m}}(t) = \frac{\Gamma_s e^{-\Gamma_s t}}{2} \left[1 \pm \cos(\Delta m_s t)\right] \;\; \Rightarrow \;\; p.d.f.^{\mathrm{u,m}}(t) = \frac{\Gamma_s e^{-\Gamma_s t}}{2} \left[1 \pm \mathcal{A}\cos(\omega t)\right] \; . \;\; (3.10)$$

The method consists in measuring $\mathcal{A}$, *i.e.*, maximizing the likelihood with respect to $\mathcal{A}$, as a function of the test frequency ω (throughout this thesis ω stands for the frequency folded in the fitting function, whereas Δm_s or Δm indicates the frequency of the oscillations in the sample studied). A value of $\mathcal{A} = 1$ is expected to be measured at $\omega = \Delta m_s$. Far below the true oscillation frequency $\mathcal{A} = 0$ is expected; a more detailed description of the expected values of the amplitude $\mathcal{A}$ as a function of the test frequency is derived in Section 3.3.2.

The idea behind the amplitude method is to define a measurable quantity, with well defined uncertainties, in such a way that an average between different analyses can be easily performed. The amplitude $\mathcal{A}$ fulfils these requirements.

The frequency range for which the amplitude is found to be compatible with zero and incompatible with one can be excluded at 95% C.L., *i.e.*,

$$\omega_0 \;\; \text{excluded at} \;\; 95\% \text{ C.L.} \;\; \text{if} \;\; \mathcal{A}_{(\omega_0)} + 1.645\,\sigma_\mathcal{A} < 1 \; . \tag{3.11}$$

The sensitivity of an analysis is defined as the expected limit at 95% C.L. given the analysis performance, *i.e.*, the limit which would be set if the measured value of $\mathcal{A}_{(\omega_0)}$ was zero. The corresponding sensitivity frequency ω^{95} fulfils,

$$\omega^{95} \;\; \Leftrightarrow \;\; 1.645 \; \times \; \sigma_{\mathcal{A}_{\omega^{95}}} \; = \; 1 \; . \tag{3.12}$$

It is equivalent to the frequency for which amplitude values zero and one can be distinguished at 95% C.L.

The amplitude $\mathcal{A}$ has well behaved parabolic uncertainties, and therefore a combination of different analyses is easily performed. A combined limit is obtained applying the above prescription to the combined amplitude scan as a function of ω.

As already mentioned, the amplitude measurements are obtained by maximizing the likelihood L of the proper time distributions of mixed and unmixed events with the amplitude of the oscillating term $\mathcal{A}$ as the free parameter, and ω fixed at a chosen value. Denote

$\mathcal{L} = -\log L$, its expansion at second order around the minimum of $\mathcal{L}$, $\mathcal{L}_\omega(\bar{\mathcal{A}})$, can be approximated by

$$\mathcal{L}_\omega(\mathcal{A}) \simeq \mathcal{L}_\omega(\bar{\mathcal{A}}) + \frac{1}{2}\left(\frac{\mathcal{A}-\bar{\mathcal{A}}}{\sigma_\mathcal{A}}\right)^2_\omega, \tag{3.13}$$

where $\bar{\mathcal{A}}$ is the measured value of the amplitude, and $\sigma_\mathcal{A}$ is the uncertainty on $\bar{\mathcal{A}}$. This approximation turns out to be very accurate in reality, $\mathcal{L}_\omega(\mathcal{A})$ being parabolic in a wide range around $\bar{\mathcal{A}}$.

From Eq. 3.13 it follows that, again for each value of ω:

$$\mathcal{L}_\omega(\mathcal{A}=1) \simeq \mathcal{L}_\omega(\bar{\mathcal{A}}) + \frac{1}{2}\left(\frac{1-\bar{\mathcal{A}}}{\sigma_\mathcal{A}}\right)^2_\omega. \tag{3.14}$$

The oscillation vanishes for $\mathcal{A} = 0$ on the one hand, and it averages to zero for $\omega \to \infty$ due to finite resolution on the other. Therefore, the following equality can be written

$$\mathcal{L}_{\omega\to\infty}(\text{any } \mathcal{A}) = \mathcal{L}_{\text{any } \omega}(\mathcal{A}=0) \; (\equiv \mathcal{L}_\infty), \tag{3.15}$$

and therefore, from Eq. 3.13,

$$\mathcal{L}_\infty = \mathcal{L}_\omega(\bar{\mathcal{A}}) + \frac{1}{2}\left(\frac{\bar{\mathcal{A}}}{\sigma_\mathcal{A}}\right)^2_\omega. \tag{3.16}$$

If Eq. 3.16 is subtracted from Eq. 3.14, the following formula is obtained

$$\Delta\mathcal{L}(\omega) \equiv \mathcal{L}_\omega(\mathcal{A}=1) - \mathcal{L}_\infty \simeq \left[\frac{1}{2}\left(\frac{1-\bar{\mathcal{A}}}{\sigma_\mathcal{A}}\right)^2 - \frac{1}{2}\left(\frac{\bar{\mathcal{A}}}{\sigma_\mathcal{A}}\right)^2\right]_\omega, \tag{3.17}$$

which allows the value of $\Delta\mathcal{L}$ to be calculated, for each ω, from the fit amplitude and its uncertainty. This formula was already given in Ref. [56] and allows a minimum of the likelihood of the world combined data (or any other combination) to be looked for.

3.3.1   Interpretation

The properties of the amplitude method for B_s oscillations were studied in detail in a paper (Ref. [9]) written by Duccio Abbaneo and myself. The three main Sections of this paper are reproduced below (some changes of notation are introduced for coherence with the rest of this thesis). In Section 3.3.2 analytical expressions for the expected shape of the measured amplitude and its uncertainty are, for the first time, derived. The small and large frequency limits are discussed, and an approximate interpretation in terms of Fourier transformations is proposed. Several mis-concepts present in the previous literature are clarified. The probability of observing statistical fluctuations which would fake a signal in a sample with the oscillation frequency far beyond the sensitivity is also discussed. In Section 3.3.3 the structure and the features of a toy-experiment generator used throughout the paper, and this thesis, are described. A procedure to tune the parameters of the simulation in order to reproduce the observed uncertainties in a particular analysis or combination of analyses is given. In
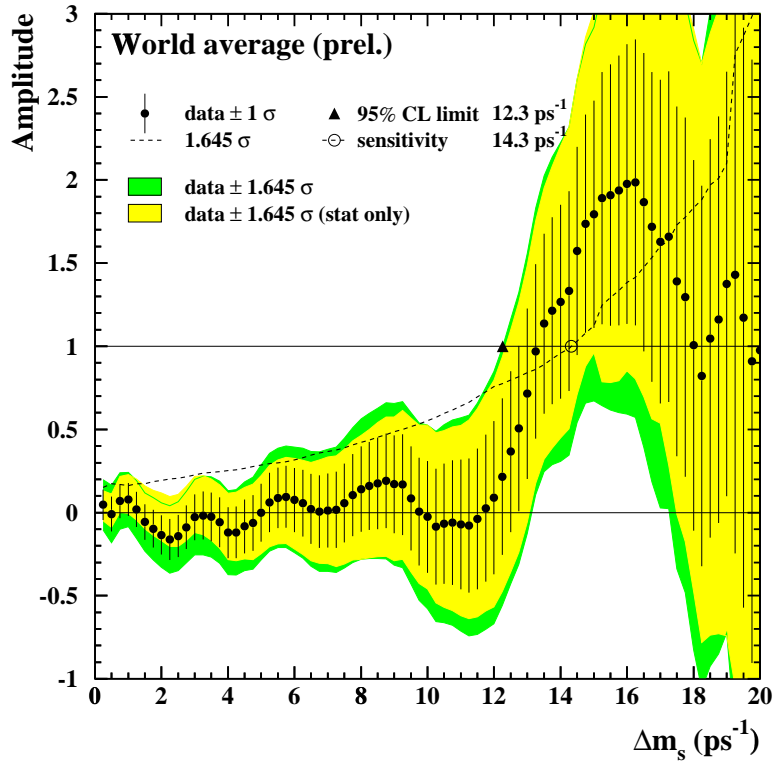
Figure 3.7: Winter 1999 combined amplitude measurements as a function of ω, from the B Oscillation Working Group.

Section 3.3.4 a procedure to extract a confidence level value from the likelihood function is presented and discussed. The uncertainty arising from the lack of a detailed simulation is investigated. The method described in this Section is used in Chapter 8 for the interpretation of the results of this thesis.

At the time of the paper publication, the latest results on B_s oscillations available were those presented in the 1999 winter conferences, and therefore these are the results used for illustration throughout the paper and in its reproduction below. For the sake of completeness, the combined amplitude measurements obtained from published and preliminary analyses available at the time of the 1999 winter conferences [8] are presented in Fig. 3.7.

The likelihood difference $\Delta\mathcal{L}(\omega)$ obtained for these data is shown in Fig. 3.8. A good parametrization for the shape of $\Delta\mathcal{L}$ is obtained with a function $f(\omega) \propto 1/\omega^\alpha$ with $\alpha = 1.64$, plus some Gaussian functions to describe the deviations. A parabolic fit of the three lowest points of the plot gives a minimum for $\omega = 14.8\,\mathrm{ps}^{-1}$, with a value $\Delta\mathcal{L}_{\min} = -2.9$. As discussed in the following sections, the significance of this minimum cannot be extracted in an analytical way, but needs to be determined with toy experiments.
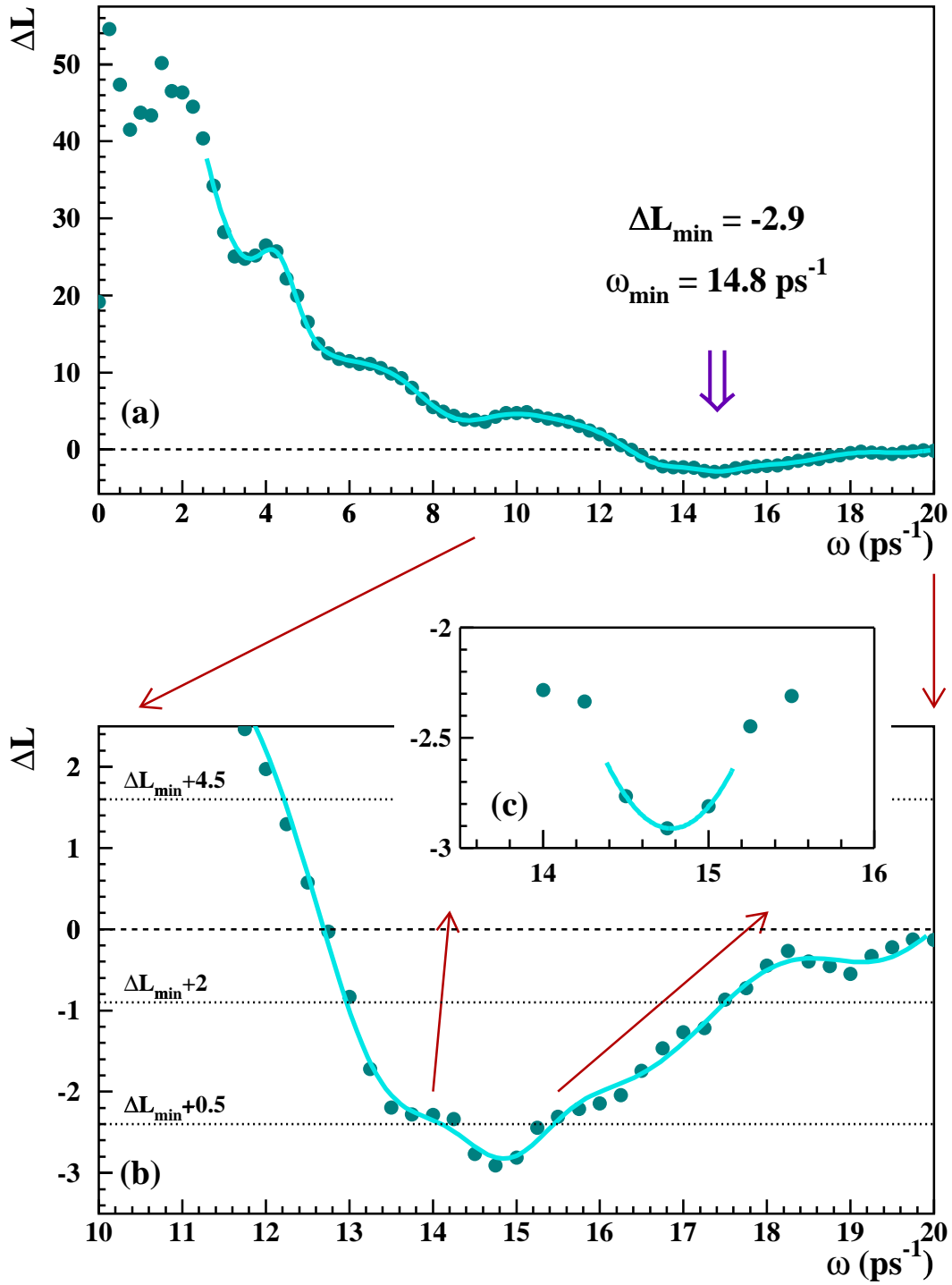
Figure 3.8: Likelihood as a function of ω derived from the combined amplitude measurements. A minimum is observed for $\omega = 14.8\,\mathrm{ps}^{-1}$. The parametrization described in the text is shown in (a) and (b); the parabolic fit to the three lowest points in (c).

3.3.2 The amplitude analysis

The true proper time distribution of mixed and unmixed B meson decays is written as follows:

$$p.d.f._{\text{u,m}}^{0}(t_0) \ = \ \Gamma \exp\left(-\Gamma t_0\right) \frac{1 \pm \cos \Delta m \, t_0}{2} \ \equiv \ \frac{E^0(t_0) \pm f_{\Delta m}^0(t_0)}{2} \, , \qquad (3.18)$$

where $f_{\Delta m}^0(t_0)$ contains the oscillation term. The plus (minus) sign holds for unmixed (mixed) events. Any difference in the decay widths of the two mass eigenstates has been neglected.

The reconstructed proper time distributions can then be written as:

$$p.d.f._{\text{u,m}}(t) \ = \ \int_0^\infty dt_0 \, \frac{E^0(t_0) \pm f_{\Delta m}^0(t_0)}{2} \, \mathcal{R}(t_0, t) \ \equiv \ \frac{E(t) \pm f_{\Delta m}(t)}{2} \, . \qquad (3.19)$$

For the sake of simplicity, no time dependent selection efficiency has been considered in the calculations. In what follows, it is assumed that the *relative uncertainty* on the b-hadron momentum, and the *absolute uncertainty* on the decay length are Gaussian. This approximation follows what typically happens in real analyses, where the uncertainty on the reconstructed b-hadron momentum is found to roughly scale with the momentum itself, while the uncertainty on the decay length does not. This fact has important consequences in the way the two resolution components affect the amplitude shape.

Under these assumptions, the resolution function $\mathcal{R}(t_0, t)$ can be written as:

$$\begin{aligned}
\mathcal{R}(t_0, t) \ &= \ \int_{-\infty}^\infty dp \, \frac{1}{\sqrt{2\pi} \, \sigma_p} \exp\left(-\frac{(p - p_0)^2}{2 \, \sigma_p^2}\right) \frac{1}{\sqrt{2\pi} \, \sigma_l} \exp\left(-\frac{(pct - p_0 ct_0)^2}{2 \, (m\sigma_l)^2}\right) \frac{pc}{m} \\
&\approx \ \frac{1}{\sqrt{2\pi \, [\delta_l^2 + (\delta_p t)^2]}} \exp\left(-\frac{(t - t_0)^2}{2 \, [\delta_l^2 + (\delta_p t)^2]}\right) \, ,
\end{aligned} \qquad (3.20)$$

where $\delta_l \equiv \sigma_l \, m/(p_0 \, c)$, $\delta_p \equiv \sigma_p/p_0$. The approximation is valid if δ_p is significantly smaller than one, which is anyway required to assume Gaussian uncertainties, since the reconstructed momentum cannot be negative. Furthermore, p_0 is not accessible in real data; the reconstructed momentum is therefore used in the evaluation of the uncertainty from the decay length resolution: $\delta_l \approx \sigma_l \, m/(p \, c)$.

A set of parameters is chosen here for the purpose of illustration. Resolution values of $\delta_p = 0.15$ and $\delta_l = 0.14 \, \text{ps}$ are used; the latter one would correspond to a monochromatic sample of B_s mesons with $p_0 = 32 \, \text{GeV}/c$ and $\sigma_l = 250 \, \mu\text{m}$. In a real analysis the normalization of the non–oscillating component is the total number N of b-hadron decays (differences in lifetime are neglected), while the oscillation term is multiplied by $N \, f_{B_s} \, (1 - 2 \, \eta_T)$, f_{B_s} being the fractions of B_s in the sample, and η_T the global mistag rate. For an inclusive analysis, $f_{B_s} \, (1 - 2 \, \eta_T)$ is typically about 0.05. The curves obtained with these parameters, normalization factors omitted, are shown in Fig. 3.9. As the frequency increases, the oscillation amplitude is damped because of the resolution. For very large frequencies only the first period can be resolved.

The fitting technique commonly used in the amplitude analysis is a simultaneous maximum–likelihood fit to the proper time distributions of mixed and unmixed events, as explained in Section 3.2. Alternatively, the difference of the two distributions, *i.e.* the oscillating term, can be fit with a binned χ^2 method. These two methods are discussed in the following.
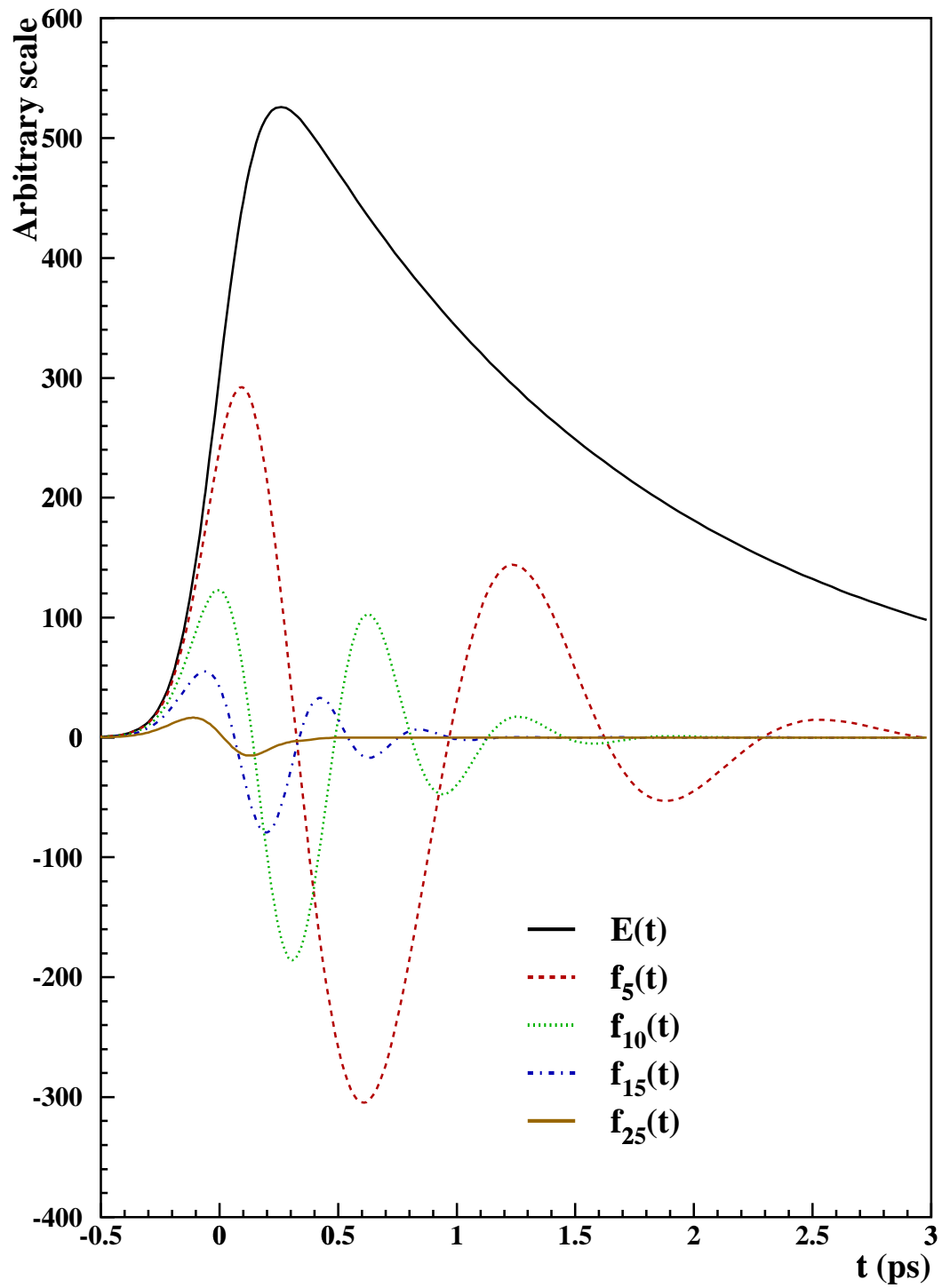
Figure 3.9: Reconstructed proper time distributions for the non–oscillating component, $E(t)$, and the oscillating component, $f_{\Delta m}(t)$, at different values of Δm. Resolutions of $\delta_p = 0.15$ and $\delta_l = 0.14\,\mathrm{ps}$ are assumed.

The maximum likelihood fit.   Using the aforementioned formalism, the likelihood function can be written as:

$$-\log L \;=\; \frac{1}{2}\int_{-\infty}^{\infty} dt \quad [E(t) + f_{\Delta m}(t)]\,\log\,[E(t) + \mathcal{A}f_\omega(t)]$$
$$+ \quad [E(t) - f_{\Delta m}(t)]\,\log\,[E(t) - \mathcal{A}f_\omega(t)] \;+\; \mathrm{Const}\,,$$

where again Δm is the frequency of the oscillations in the sample analysed, and ω is the value chosen in the fitting function. The minimization with respect to $\mathcal{A}$ leads to the condition

$$\int_{-\infty}^{\infty} dt \; \frac{f_\omega(t)\,f_{\Delta m}(t) - \mathcal{A}f_\omega^2(t)}{E(t)\left(1 - \mathcal{A}^2 \frac{f_\omega^2(t)}{E^2(t)}\right)} \;=\; 0\,, \tag{3.21}$$

which allows $\mathcal{A}$ to be determined.

The χ^2 fit.   Similarly, the χ^2 can be written as

$$\chi^2 \;=\; \int_{-\infty}^{\infty} dt \; \frac{[f_{\Delta m}(t) - \mathcal{A}f_\omega(t)]^2}{E(t)}\,, \tag{3.22}$$

the minimization of which gives

$$\int_{-\infty}^{\infty} dt \; \frac{f_\omega(t)\,f_{\Delta m}(t) - \mathcal{A}f_\omega^2(t)}{E(t)} \;=\; 0. \tag{3.23}$$

Equations 3.21 and 3.23 both give $\mathcal{A} = 1$ for $\omega = \Delta m$. For $\omega \neq \Delta m$ they are equivalent if $\mathcal{A}f_\omega(t)$ is negligible compared to $E(t)$.

The expression of $\mathcal{A}_{\Delta m}(\omega)$ can be derived from Eq. 3.23 as

$$\mathcal{A}_{\Delta m}(\omega) \;=\; \frac{\displaystyle\int_{-\infty}^{\infty} dt \; \frac{f_\omega(t)\,f_{\Delta m}(t)}{E(t)}}{\displaystyle\int_{-\infty}^{\infty} dt \; \frac{f_\omega^2(t)}{E(t)}}\,. \tag{3.24}$$

The resulting amplitude curves for $\Delta m = 5,\ 10,\ 15\ \mathrm{ps}^{-1}$ are shown in Fig. 3.10a. On top of the curves, values obtained from the likelihood fit (Eq. 3.21) are also shown. The two fitting methods are indeed equivalent for $\omega \approx \Delta m$, as expected, while some difference appears for $\omega \neq \Delta m$.

The expected amplitude is unity at $\omega = \Delta m$. For $\omega > \Delta m$, the behaviour depends on Δm (for given resolutions). In this example, for $\Delta m = 15\,\mathrm{ps}^{-1}$ the expected amplitude increases monotonically.

The expressions derived for the χ^2 fit allow also the expected uncertainty on the measured amplitude to be extracted,

$$\chi^2(\mathcal{A} + \sigma_\mathcal{A}) - \chi^2(\mathcal{A}) \;=\; 1, \tag{3.25}$$

which in turn gives

$$\sigma_\mathcal{A}(\omega) \;=\; \frac{1}{\sqrt{\displaystyle\int_{-\infty}^{\infty} dt \; \frac{f_\omega^2(t)}{E(t)}}}\,. \tag{3.26}$$
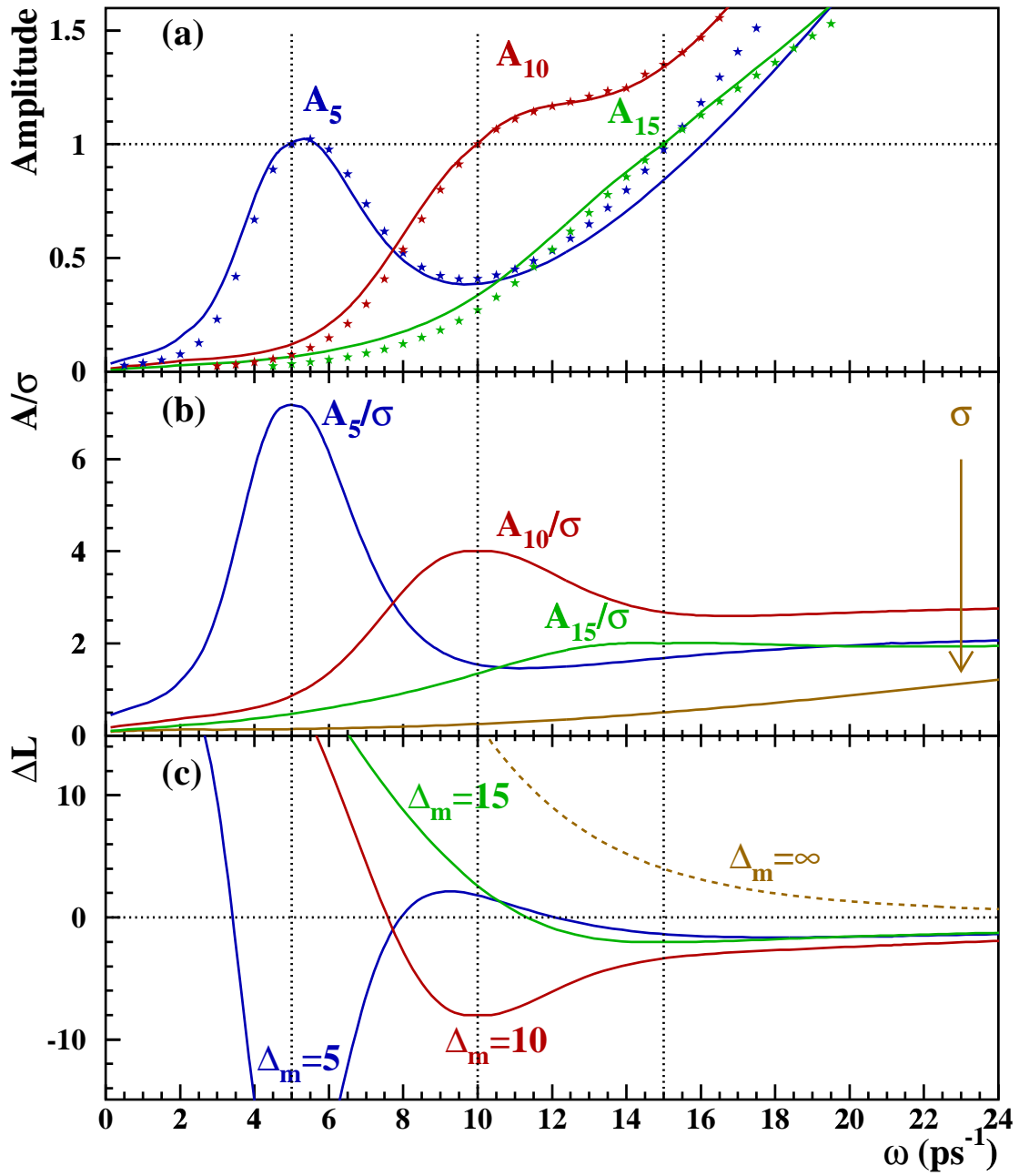
Figure 3.10: (a) Expected amplitude values for $\Delta m = 5, 10, 15,$ ps^{-1}. The curves refer to the χ^2 minimization, the points to the likelihood fit.

(b) Amplitude significance curves (χ^2 fit). The expected shape of $\sigma(\omega)$ is also shown.

(c) Expected shape of the likelihood, derived from the amplitude and its uncertainty. The dashed line corresponds to the the limit $\Delta m \rightarrow \infty$.

Resolutions of $\delta_p = 0.15$ and $\sigma_l = 250 \, \mu$m are assumed for the three plots.

If a global mistag probability η_T, and the B_s signal fraction in the data f_s are introduced, the expression for the amplitude curve remains unchanged, but the expected uncertainty on the amplitude becomes, for a statistics of N events,

$$\sigma_{\mathcal{A}}^{-1}(\omega) \;=\; \sqrt{N}\,(1 - 2\eta_T)\,f_s\,\sqrt{\int_{-\infty}^{\infty} dt\;\frac{f_\omega^2(t)}{E(t)}}\;. \tag{3.27}$$

The significance of the measured amplitude is therefore:

$$S_{\Delta m}(\omega) \;=\; \frac{\mathcal{A}_{\Delta m}(\omega)}{\sigma_{\mathcal{A}}^{\Delta m}(\omega)} \;=\; \frac{\displaystyle\int_{-\infty}^{\infty} dt\;\frac{f_\omega(t)\,f_{\Delta m}(t)}{E(t)}}{\sqrt{\displaystyle\int_{-\infty}^{\infty} dt\;\frac{f_\omega^2(t)}{E(t)}}}\;\sqrt{N}\,(1 - 2\eta_T)\,f_s\;. \tag{3.28}$$

This latter equation is correct only because $\mathcal{A}$ and $\sigma_{\mathcal{A}}$ are independent.

The amplitude significance curves for $\Delta m = 5,\ 10,\ 15\,\text{ps}^{-1}$ are shown in Fig. 3.10b. The normalization of the uncertainty, in the same figure, is arbitrarily chosen to have $\sigma_{\mathcal{A}} = 0.5$ at $\omega = 15\,\text{ps}^{-1}$.

The expected significance is maximal at $\omega = \Delta m$. For $\omega > \Delta m$ it decreases without reaching zero in the range explored. The decrease is more smooth for high values of Δm.

The expected shape of the likelihood, as calculated from the amplitude and its uncertainty using Eq. 3.17, is shown in Fig. 3.10c.

Limits for small and large Δm

In the limit of very small or very large Δm, some approximations can be made in the formulae, which yield simplified expressions of easier interpretation.

Small Δm. If $\delta_l \ll 1/\Delta m$, $\delta_p/\Gamma \ll 1/\Delta m$, the oscillation is slow and marginally affected by the resolution. This limit holds in the case of B_d oscillations. If the resolution effects are neglected, Eq. 3.24 can be rewritten as

$$\mathcal{A}_{\Delta m}(\omega) \;=\; \frac{\displaystyle\int_0^{\infty} dt\;\Gamma \exp(-\Gamma t)\,\cos\omega t\,\cos\Delta m t}{\displaystyle\int_0^{\infty} dt\;\Gamma \exp(-\Gamma t)\,\cos^2\omega t}\;, \tag{3.29}$$

which gives

$$\mathcal{A}_{\Delta m}(\omega) \;\approx\; \frac{\dfrac{\Gamma^2}{\Gamma^2 + (\omega + \Delta m)^2} + \dfrac{\Gamma^2}{\Gamma^2 + (\omega - \Delta m)^2}}{1 + \dfrac{\Gamma^2}{\Gamma^2 + 4\,\omega^2}}\;. \tag{3.30}$$

The resulting shape is shown in Fig. 3.11. The dots superimposed are obtained with toy experiments generated at the same value of the frequency, including resolution effects (for details on the simulation see Section 3.3.3; the parameters used in the generation are those of samples **S** there defined). The two shapes are in qualitatively good agreement.
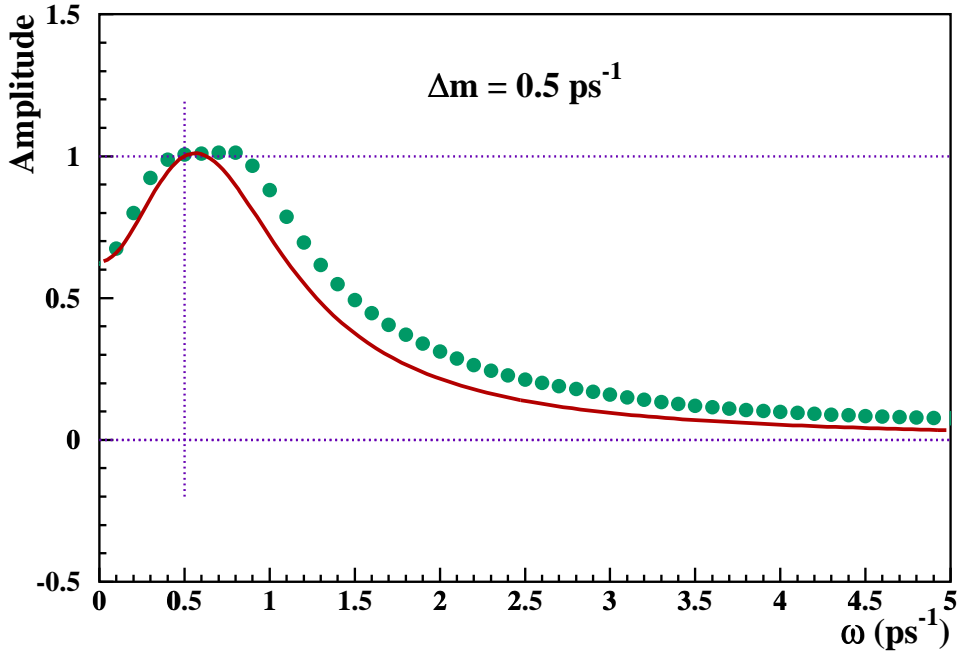
Figure 3.11: The full curve gives the expected shape of the amplitude for a signal at $\Delta m = 0.5\,\mathrm{ps}^{-1}$ when all resolution effects are neglected. The dots are obtained with a toy experiment in which resolution effects are simulated (where $\delta_p = 0.15$ and $\sigma_l = 250\,\mu\mathrm{m}$). The two shapes are in agreement.

Large Δm. In this limit, which corresponds to the regime of B_s oscillations, the resolution effects dominate. If $\Delta m_s \approx 15\,\mathrm{ps}^{-1}$ and $\delta_p = 0.15$, then $\delta_p/\Gamma \simeq 0.23\,\mathrm{ps}$, which is larger than $1/\Delta m_s \approx 0.07\,\mathrm{ps}$ and therefore implies that only events with small proper time contribute to the sensitivity. Similarly, taking $\delta_l = 0.14\,\mathrm{ps}$ gives $\delta_l > 1/\Delta m_s$, which implies a substantial damping of the amplitude of the oscillating term due to the decay length resolution. In this case, a useful approximation is to assume that the term $E(t)$ in Eq. 3.24 varies slowly compared to the fast oscillating term $f_\omega(t)$, which is non-zero in a limited time range (Fig. 3.9), and take it out of the integral. In this way the expression can be simplified and rewritten in terms of the Fourier transformation of the oscillating components,

$$
\mathcal{A}_{\Delta m}(\omega) \;\approx\; \frac{\int_{-\infty}^{\infty} dt\; f_\omega(t)\, f_{\Delta m}(t)}{\int_{-\infty}^{\infty} dt\; f_\omega^2(t)} \;=\; \frac{\int_{-\infty}^{\infty} d\nu\; \tilde{\mathrm{f}}_\omega(\nu)\, \tilde{\mathrm{f}}_{\Delta m}(\nu)}{\int_{-\infty}^{\infty} d\nu\; \tilde{\mathrm{f}}_\omega^{\,2}(\nu)}\;.
\tag{3.31}
$$

The approximation is valid only if both ω and Δm are large. The functions $\tilde{\mathrm{f}}_\omega$ are shown in Fig. 3.12a for a few different values of $\omega \geq 10\,\mathrm{ps}^{-1}$. Fig 3.12c shows the product of two of these Fourier transformations to illustrate the behaviour of the ratio in Eq. 3.31.

With increasing Δm, the frequency spectra, $\tilde{\mathrm{f}}_\omega$, become broader and smaller in amplitude. High *true* frequencies, Δm, have their spectrum damped faster than low frequencies, and the peak at $\omega \approx \Delta m$ disappears for Δm well beyond the sensitivity (Fig. 3.12b). Due to the broadening of the spectra, the product $\tilde{\mathrm{f}}_{\omega_1}(\nu)\tilde{\mathrm{f}}_{\omega_2}(\nu)$ is peaked around the smallest between
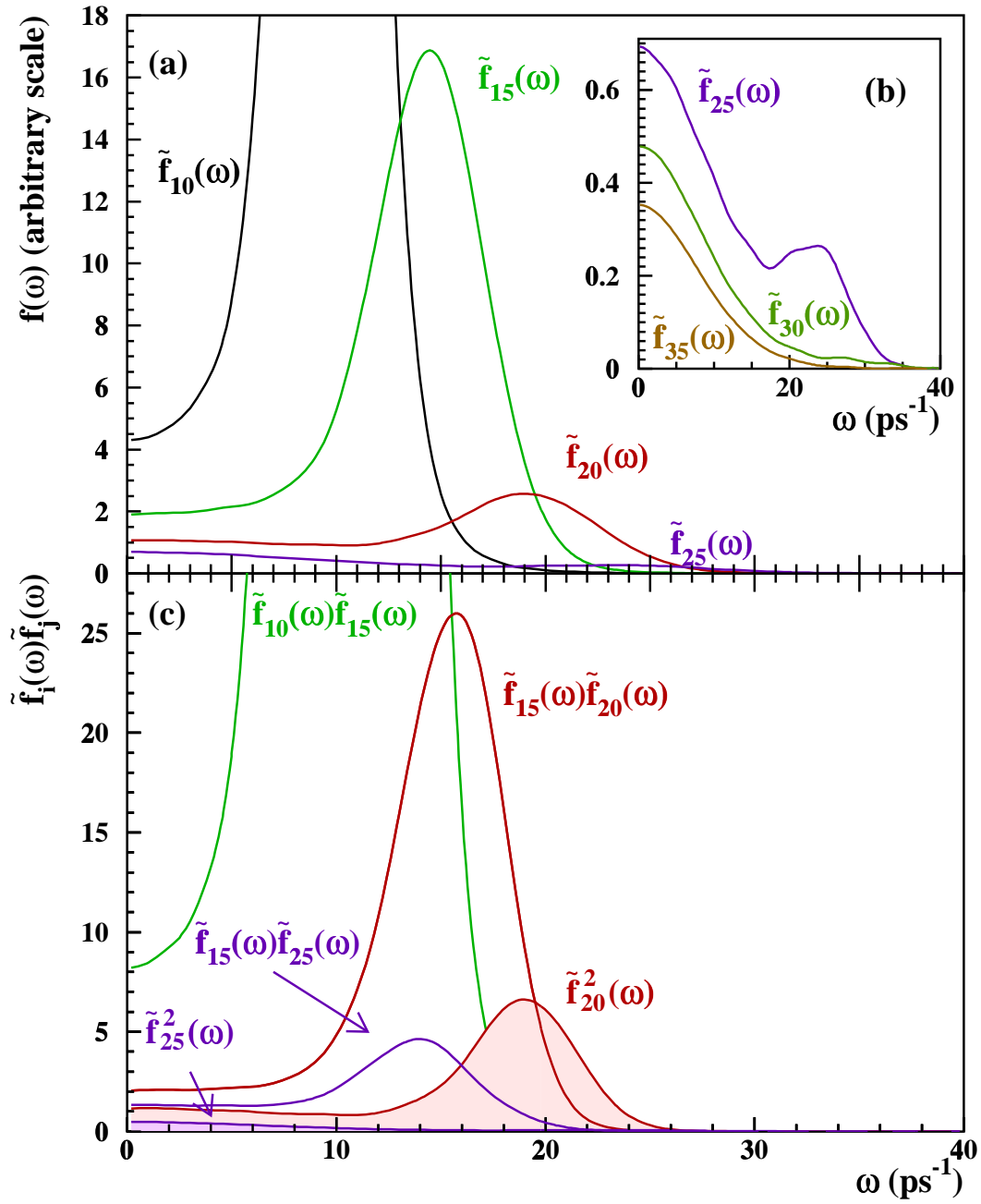
Figure 3.12: (a) Expected shapes of the Fourier spectra $\tilde{\mathrm{f}}_{\Delta m}$ for different values of Δm. The spectra become broader and lower in amplitude when Δm increases.

(b) Detail of the spectra for high Δm.

(c) Products of pairs of Fourier spectra. The resulting functions are peaked around the smallest of the two frequency values.

Resolutions of $\delta_p = 0.15$ and $\sigma_l = 250\,\mu$m are assumed.

ω_1 and ω_2 (Fig. 3.12c). This fact implies that when a sample with oscillations at frequency Δm is analysed with a function containing a frequency $\omega < \Delta m$, the measured amplitude is dominated by the frequencies around ω; therefore the shape of $\mathcal{A}_{\Delta m}(\omega)$ for $\omega < \Delta m$ resembles that of $\tilde{f}_{\Delta m}(\omega)$. For $\omega > \Delta m$ the frequencies around Δm are always tested, with a normalization factor which increases with ω (in Eq. 3.31, the denominator decreases very fast), therefore $\mathcal{A}_{\Delta m}(\omega)$ increases monotonically.

In order to understand better the effect of the decay length and proper time resolution, it is useful to study them separately. Setting $\delta_p = 0$ in Eq. 3.20, the following simplified expression can be obtained,

$$\tilde{f}_{\Delta m}(\omega) \;=\; \frac{1}{2}\left[\frac{\Gamma^2}{\Gamma^2 + (\omega + \Delta m)^2} + \frac{\Gamma^2}{\Gamma^2 + (\omega - \Delta m)^2}\right]\exp\left(-\frac{\delta_l^2\omega^2}{2}\right), \qquad (3.32)$$

which shows that the decay length resolution is responsible for the damping of the high frequencies.

Considering the momentum resolution alone, the following expression is obtained,

$$\tilde{f}_{\Delta m}(\omega) \;=\; \int_{-\infty}^{\infty} d\nu\;\frac{1}{2}\left[\frac{\Gamma^2}{\Gamma^2 + (\nu + \Delta m)^2} + \frac{\Gamma^2}{\Gamma^2 + (\nu - \Delta m)^2}\right]\exp\left(-\frac{(\omega - \nu)^2}{2\,(\delta_p\omega)^2}\right), \quad (3.33)$$

which shows that the momentum resolution causes the broadening of the frequency spectrum (as intuitively expected, since a shift in the reconstructed momentum is equivalent to a change of scale on the time axis). For $\Delta m = 15\,\text{ps}^{-1}$ and $\delta_p = 0.15$, the width of the frequency spectrum is dominated by the momentum resolution.

A broader frequency spectrum corresponds to a broader structure in the amplitude spectrum, or, equivalently, to higher correlations between values of the amplitude measured at different frequencies. This property is relevant for the confidence level estimation as explained in Section 3.3.4.

Fluctuations

The expected shape of the likelihood for a sample with oscillations at a frequency far beyond the sensitivity is shown in Fig. 3.10c. In a given frequency range, statistical fluctuations of the likelihood can produce values below 0 which can fake a signal. The probability of observing that $\Delta\mathcal{L}$ is lower than a given value $\overline{\Delta\mathcal{L}}$ at a given frequency ω can be estimated from Eq. 3.17, using the fact that the uncertainties on the measured amplitudes are found to be Gaussian with high precision:

$$\mathcal{P}(\Delta\mathcal{L}, \omega) \;\equiv\; \mathcal{P}(\Delta\mathcal{L} < \overline{\Delta\mathcal{L}})_\omega \;=\; \frac{1}{2}\,\text{erfc}\left[\left(-\overline{\Delta\mathcal{L}}\,\sigma_{\mathcal{A}}(\omega) + \frac{1}{2\,\sigma_{\mathcal{A}}(\omega)}\right)\Big/\sqrt{2}\right]. \qquad (3.34)$$

The function $\mathcal{P}(\Delta\mathcal{L}, \omega)$ is shown in Fig 3.13a, where the same parameters and normalization as for Fig. 3.10 are used. This function can be used as an estimator of the signal–ness of a given sample. Estimator contours, equidistant on a logarithmic scale, are drawn in Fig. 3.13b. Small negative values are most probable at high frequencies, while for larger negative values the maximum of the probability is found at lower frequencies.
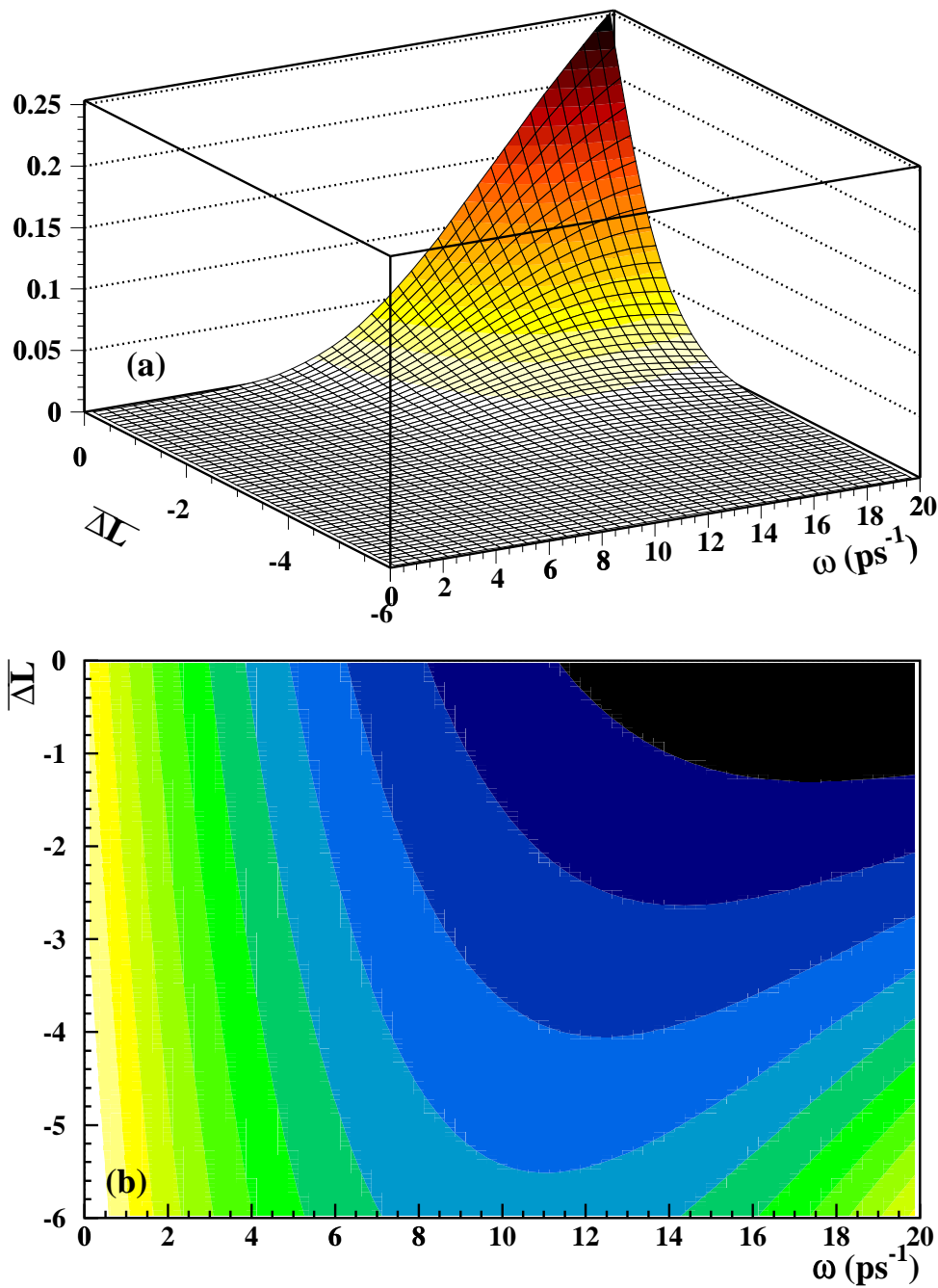
Figure 3.13: (a) Probability to find a $\Delta\mathcal{L}$ value lower than $\overline{\Delta\mathcal{L}}$ at a frequency ω. (b) Contours of equal probability in the $(\overline{\Delta\mathcal{L}}, \omega)$ plane. Values between -3 and -5 are found with higher probability when the uncertainty on the amplitude is from 0.5 (at $\omega = 15\,\mathrm{ps}^{-1}$ in this example) to 0.3 ($\omega \approx 11\,\mathrm{ps}^{-1}$). The contours shown are equidistant on a logarithmic scale.
Resolutions of $\delta_p = 0.15$ and $\delta_l = 0.14\,\mathrm{ps}$ are assumed.

3.3.3   The toy experiments

The probability that the minimum observed in the likelihood (Fig. 3.8) is caused by a fluctuation can be evaluated by means of toy experiments with the above estimator (Eq. 3.34).

In a general case, the depth of the likelihood minimum can be translated to a statistical significance in the approximation that the likelihood is parabolic, which is not the case here.

At each frequency point, the probability that the measured $\Delta\mathcal{L}$ is lower than a given value $\overline{\Delta\mathcal{L}}$ can be calculated as explained in Section 3.3.2, starting from the uncertainties on the measured amplitude. This procedure cannot be applied to the minimum, since $\Delta\mathcal{L}_{\min}$ is not an "unbiased" value, but it is chosen as the lowest value found over a certain frequency range explored.

The sum of the probabilities of obtaining a likelihood value lower than observed at all points where the amplitude is measured does not provide a good estimate either. The different points are highly correlated and they cannot fluctuate independently, therefore the sum of the individual probabilities would give a gross overestimate of the overall probability of finding a minimum as or more unlikely than the one observed.

The only viable possibility is to calibrate the significance of the structure observed with the help of toy experiments. The worldwide combination includes many analyses, and a detailed simulation of each of them is highly impractical. The procedure adopted here is to choose a set of parameters for the generation of the toy experiments such that each experiment is equivalent to the world average. The set of parameters cannot be uniquely determined from the data: it turns out that some parameters need to be fixed *a priori*, and therefore the dependence of the result obtained upon the particular choice adopted needs to be understood. The possible effects of the lack of a detailed simulation are investigated in Section 3.3.4 by studying the dependence of the correlations in the amplitude measurements upon the parameters chosen to generate the toy experiments.

Generation

The basic features of the toy experiments used to estimate the significance of the likelihood minimum can be summarized as follows.

- Bottom hadron species are generated according to a chosen composition.

- For each species, the *true* proper time t_0 of each b-hadron is generated according to an exponential with decay constant equal to its width, Γ, multiplied by a given efficiency function.

- Neutral B mesons are allowed to mix. Mixed and unmixed particles have their proper time distributions modified by the appropriate oscillating term, with given frequency.

- The *true* momentum p_0 is generated according to a Peterson distribution, tuned to reproduce a given mean scaled energy $\langle x_b \rangle$.

- The *true* decay length is then obtained, for each b-hadron, from

$$l_0 \,=\, \frac{t_0\, p_0}{m}\, c\,.$$

- A smearing is applied to the *true* decay length and momentum according to given resolution functions, to obtain the *measured* decay length and momentum, l and p.

- The *measured* proper time is hence calculated as

$$t = \frac{l\,m}{p\,c}\,.$$

- A mixed/unmixed tag is assigned to the generated hadrons using specified mistag rates.

- The udsc background is neglected.

The choice of the parameters

The only information, at the level of the world combination, which can drive the choice of the parameters for the simulation is provided by the uncertainty on the measured amplitude as a function of the frequency ω. The step (seen in Fig. 3.7) at $\omega = 15\,\mathrm{ps}^{-1}$ is due to some analyses in which the scan was not performed beyond that value of the frequency. The step at $\omega = 19\,\mathrm{ps}^{-1}$ is due to the SLD analyses, for which no measurement was provided for $\omega > 19\,\mathrm{ps}^{-1}$. In all what follows the four points with $\omega > 19\,\mathrm{ps}^{-1}$ are ignored, in order to reduce the pathologies in the uncertainty shape.

The uncertainties on the measured amplitudes can be formally written as (see also Eq. 3.27)

$$\sigma_{\mathcal{A}}^{-1}(\omega) \;=\; \sqrt{N}\,f_{\mathrm{B_s}}\,(1 - 2\,\eta_T)\,\Sigma(\delta_p, \sigma_l, \omega)\,. \tag{3.35}$$

The factor $\kappa = \sqrt{N}\,f_{\mathrm{B_s}}\,(1 - 2\,\eta_T)$ gives the normalization of the uncertainty distribution, without affecting the shape, and obviously the three parameters can not be disentangled. It is chosen to fix $f_{\mathrm{B_s}}$ and η_T to some "typical" values (namely $f_{\mathrm{B_s}} = 0.15$, $\eta_T = 0.25$), and adjust N to fit the uncertainties in the data. The effect of a different choice which yields the same κ value is investigated in Section 3.3.4.

The decay length and momentum resolution terms both affect the shape of the measured uncertainty as a function of ω. The sensitivity is not enough to get a reliable simultaneous determination of both. It is thus chosen to fix δ_p, again, to a "typical" value of $\delta_p = 0.15$, and tune the value of σ_l. This choice is preferred because, as explained later, δ_p plays an important rôle in the determination of the confidence level, and needs anyway to be varied over a wide range to check the stability of the result obtained.

Samples are generated at three starting points for σ_l, which are chosen to be $200\,\mu\mathrm{m}$, $250\,\mu\mathrm{m}$ and $300\,\mu\mathrm{m}$, each with 30000 events and the other parameters as described above.

For each value of σ_l, the number of events in the toy experiments is tuned by minimizing the sum of the differences with the data uncertainties,

$$\sum_i \left(\sigma_{\mathcal{A}}^{\mathrm{data}} - \sigma_{\mathcal{A}}^{\mathrm{toy}} \right)_i^2 \,, \tag{3.36}$$

where the scaling low of Eq. 3.35 is used (Fig. 3.14a). The three minima found are then compared and interpolated with a parabolic fit (Fig. 3.14b) to find the absolute minimum, which turns out to be very close to $250\,\mu\mathrm{m}$. The number of events needed at this point is 34000.
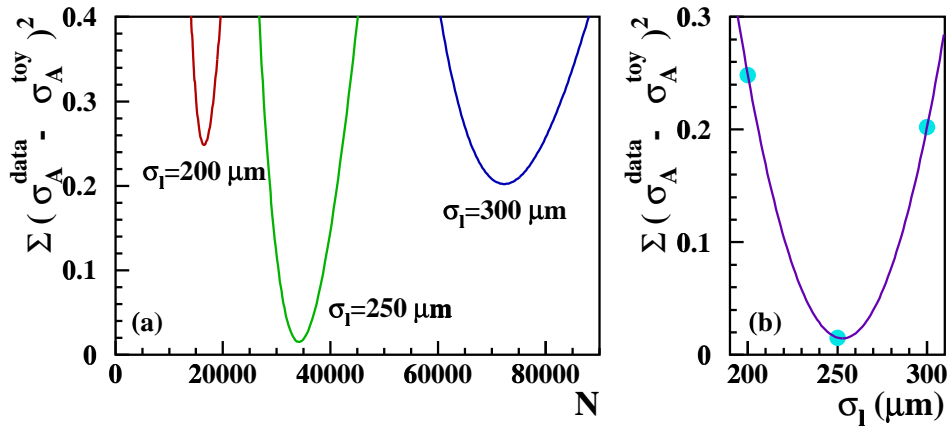
Figure 3.14: (a) Optimization of the number of events for three different values of the decay length resolution.
(b) Choice of the optimal decay length resolution.

Samples description

On the basis of the procedure described above, a set of parameters **S** is defined as follows:

- a single *purity* class: $15\%\,B_s$ $38\%\,B_d$ $38\%\,B^+$ $9\%\,\Lambda_b$;

- a single *tagging* class: mistag rate $\eta_T = 25\%$ for all species;

- a single *resolution* class:

$$\left.\begin{array}{l} \sigma_l = 250\,\mu\mathrm{m} \\ \sigma_p/p_0 = 0.15 \end{array}\right\} \text{ both Gaussian with no tails;}$$

- Monte Carlo parametrized efficiency (taken from the analysis of Ref. [10]). The curve is shown in Fig. 3.15;

- b-hadron masses and lifetimes, and Δm_d from Ref. [13];

- $\langle x_b \rangle = 0.7$;

- Δm_s fixed at different values, according to the study considered;

- statistics of 34000 b-hadron decays.

A second set of parameters **S'** is defined to generate a second family of toy experiments. The momentum resolution is chosen to be $\sigma_p/p_0 = 0.07$, which is significantly better than what is typically achieved in inclusive analyses. In order to keep the agreement with the world average uncertainties on the measured amplitudes, the number of events is reduced to 29000 (obtained with the procedure described above). The other parameters are left unchanged. These experiments are used in the following to investigate the dependence of the confidence level upon the momentum resolution.
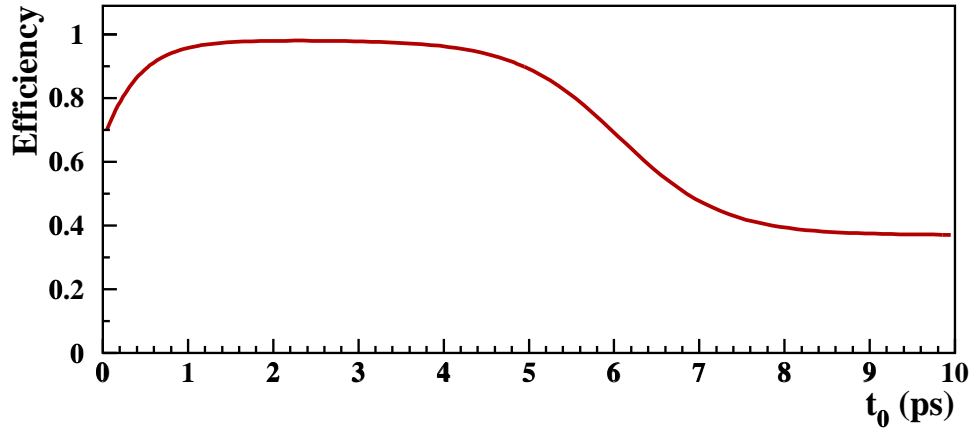
Figure 3.15: Shape of the reconstruction efficiency as a function of true proper time. The normalisation of the vertical scale is arbitrary.
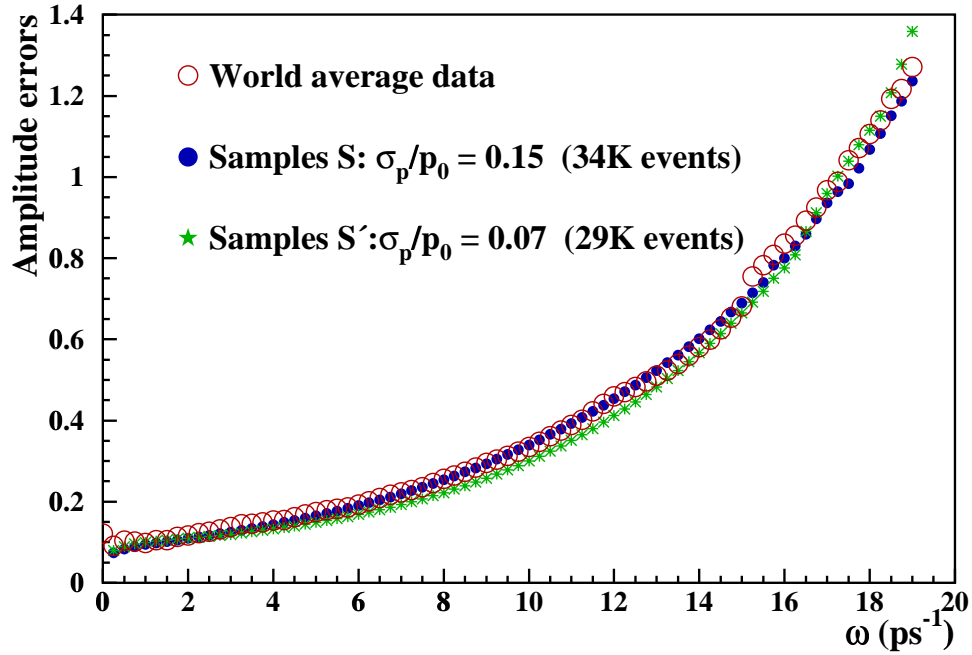

Figure 3.16: Amplitude uncertainties comparison: simulated experiments *versus* world average data.

The uncertainties on the amplitude, $\sigma_{\mathcal{A}}$, obtained with these two sets of experiments are compared to the uncertainties from the world combined data in Fig. 3.16. The step at $\omega = 15\,\mathrm{ps}^{-1}$ could be reproduced by averaging, for each "experiment", two "analyses", of which one has its scan stopped at that point. No attempt was made in this direction.

A third set of samples $\mathbf{S}''$ with $\delta_p = 0.15$, $\sigma_l = 200\,\mu\mathrm{m}$ and statistics of 16500 decays (which correspond to the optimization of Fig. 3.14) is used to investigate the dependence of
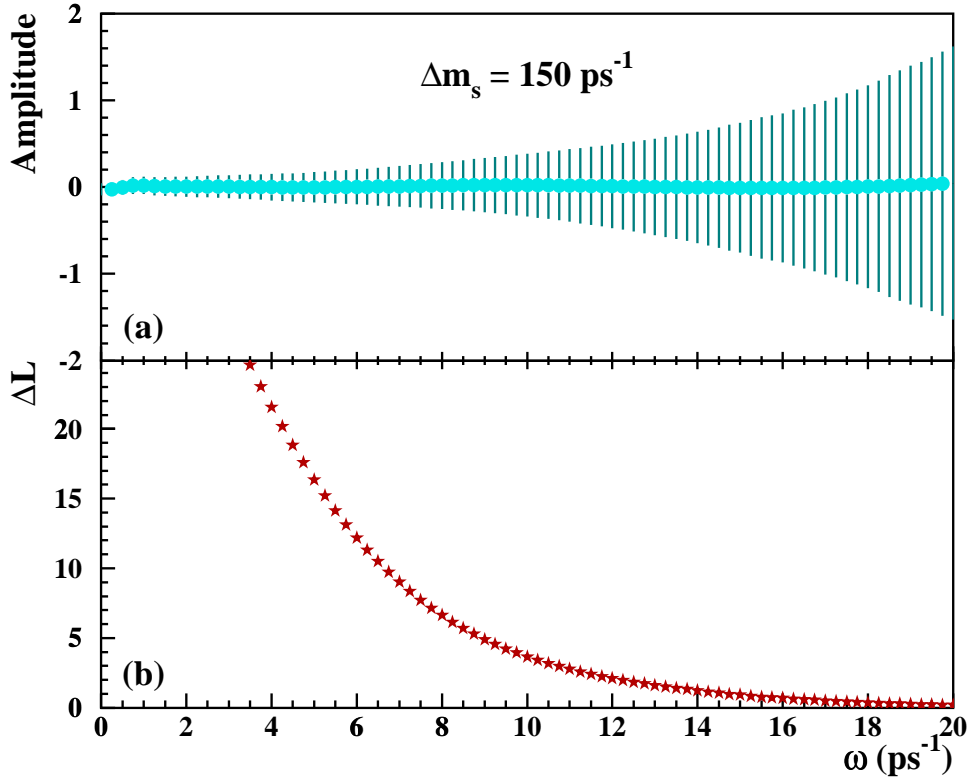
Figure 3.17: (a) Expected amplitude and uncertainty for samples of type **S**, with $\Delta m_{\mathrm{s}} = 15\,\mathrm{ps}^{-1}$, as a function of ω.
(b) Expected likelihood shape. The plots are obtained by averaging 2000 samples. Resolutions of $\delta_p = 0.15$ and $\sigma_l = 250\,\mu\mathrm{m}$ are assumed.

the confidence level upon the decay length resolution.

Finally samples of type **s** are defined from samples **S** by increasing $f_{\mathrm{B_s}}$ by a factor of five (*i.e.*, having $f_{\mathrm{B_s}} = 0.75$) and reducing the statistics by a factor of 25 (which gives 1360 decays).

In Fig. 3.17 the expected shape of the amplitude and the likelihood is shown, as obtained by averaging 1000 samples of type **S**, generated with $\Delta m_{\mathrm{s}} = 150\,\mathrm{ps}^{-1}$. The expected value is consistently zero, and the uncertainties on $\mathcal{A}$ are Gaussian, which confirms the validity of the amplitude method to set limits on the oscillation frequency.

3.3.4   The estimate of the significance

As demonstrated in Section 3.3.2, the probability that, at a given point in the frequency scan, a value of the likelihood $\Delta\mathcal{L} < \overline{\Delta\mathcal{L}}$ be found, can be calculated, given $\overline{\Delta\mathcal{L}}$, from the uncertainty on the measured amplitude, which is available from the data.

For the purpose of establishing the significance of the minimum, however, this probability is not enough, since what is needed is the probability that anywhere in the range explored

a configuration more unlikely than the one observed may appear (in the hypothesis of large Δm_{s}). This significance is driven not only by the uncertainties, but also by the correlations between the amplitude measurements at different frequencies, which are not controlled from the data, and might depend on the particular combination of parameters chosen for the simulation. It is therefore mandatory to identify the most relevant sources of systematic uncertainty which might affect the extraction of the confidence level. This point is investigated in what follows.

Correlations

From the discussion of Section 3.3.2, it turns out that the momentum resolution is the most critical parameter to determine the point–to–point correlation in the amplitude scan. In a sample with better momentum resolution, correlations are smaller and therefore the probability of having significant deviations from $\mathcal{A} = 0$ in a sample with no signal is larger, in a given frequency range explored.

In order to investigate the dependence of the point–to–point correlation upon the parameters used in the generation, a sensitive quantity is the average difference between amplitudes measured at two given points in the frequency scan. If there were no correlations, this difference could be written in terms of the uncertainties on the amplitude as

$$\langle\, |\, \mathcal{A}_i - \mathcal{A}_j\, |\, \rangle \;=\; \sqrt{\frac{2}{\pi}}\, \sqrt{\sigma_{\mathcal{A}}^{i}{}^{2} + \sigma_{\mathcal{A}}^{j}{}^{2}}\;. \tag{3.37}$$

Correlations reduce this value if i and j are close enough. A scan in steps of $0.25\,\mathrm{ps}^{-1}$ is assumed, as for the data analyses.

For each of the four set of parameters, $\mathbf{S}$, $\mathbf{S'}$, $\mathbf{S''}$ and $\mathbf{s}$ defined in Section 3.3.3, 150 samples are produced, and the quantity $\langle\, |\, \mathcal{A}_i - \mathcal{A}_j\, |\, \rangle$ is calculated, for $i - j = 1,\ 4,\ 7,\ 10$. The results are shown in Fig. 3.18, where they are compared with the expectation for no point–to–point correlation.

Compared to the most "realistic" samples, $\mathbf{S}$, the largest deviation is observed, as expected, when the momentum resolution is changed (samples $\mathbf{S'}$). At low ω, the difference between the no-correlation limit (curve) and the values found in the simulation (markers), decreases rapidly as the distance between the points increases: for $i-j = 4\ (\Leftrightarrow \Delta\omega = 1\,\mathrm{ps}^{-1})$ it is reduced by about a factor of two compared to $i - j = 1$, so $\Delta\omega = 1\,\mathrm{ps}^{-1}$ can be taken as an estimate of the "correlation length" at small frequencies. When ω increases, the difference between the curve and the simulation remains substantial even when the points are a few inverse pico-seconds apart, demonstrating the increase of the correlation length with ω.

Samples $\mathbf{S'}$ can be used to estimate a "systematic uncertainty" on the confidence level obtained, coming from the specific choice of the parameters used in the simulation.

The Confidence Level

The significance of the minimum observed in the $\Delta\mathcal{L}$ distribution (Fig. 3.8) is estimated by computing the probability that a structure as or more unlikely is observed in a sample with Δm_{s} far beyond the sensitivity.
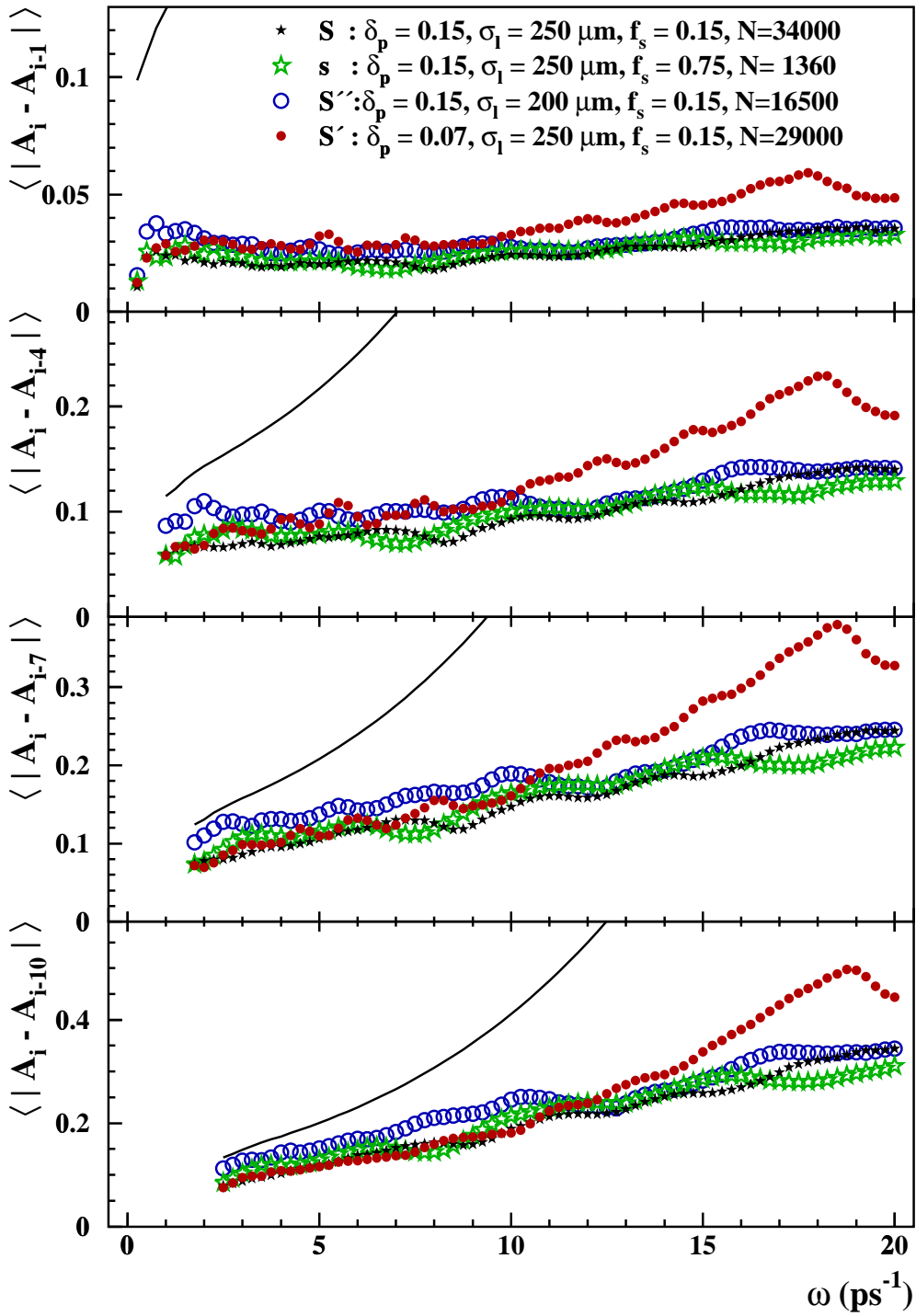
Figure 3.18: Point–to–point fluctuations for four sets of samples. From top to bottom, the average difference between points distant 1–4–7–10 steps in the amplitude scan are shown. The lines correspond to the limit of no correlation between points.
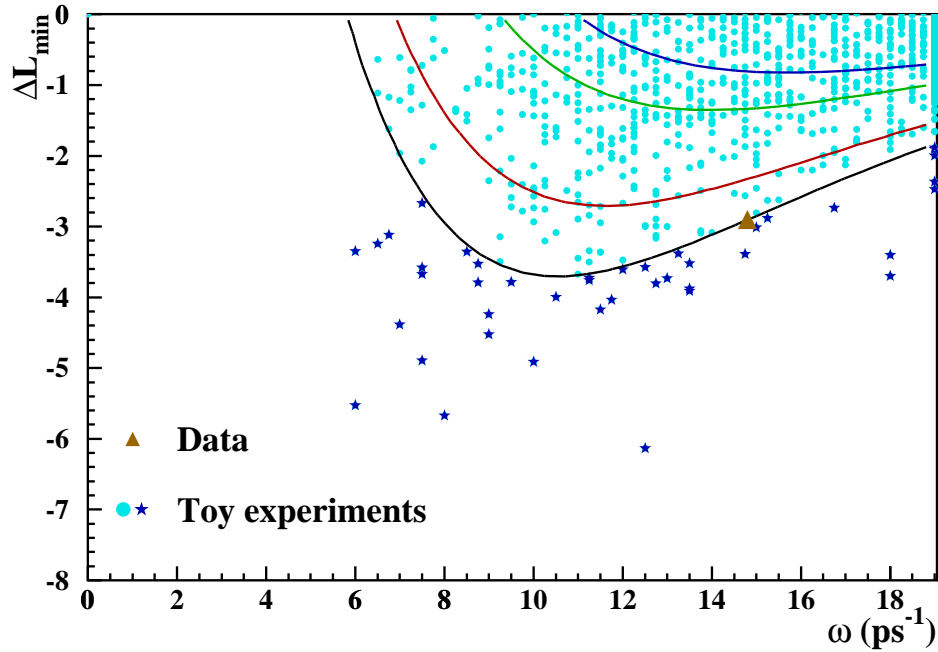
Figure 3.19: Minima of $\Delta\mathcal{L}$ for 2000 samples of type **S**, with $\Delta m_{\mathrm{s}} = 150\,\mathrm{ps}^{-1}$. The curves represent contours of equal probability of observing a value of $\Delta\mathcal{L}$ smaller than $\overline{\Delta\mathcal{L}}$, as a function of ω (as in Fig. 3.13).

In order to do that, it is taken into account that the probability of observing a given value of $\Delta\mathcal{L}$ is a non–trivial function of ω. Probability contours in the $(\Delta\mathcal{L}, \omega)$ plane (as in Fig. 3.13b) are built from the data uncertainties. The contour corresponding to the data sample is computed. $N = 2000$ samples of type **S** with $\Delta m_{\mathrm{s}} = 150\,\mathrm{ps}^{-1}$ are analysed and the number $N_{\mathrm{exp}}^{\mathrm{out}}$ of those that give a minimum $\Delta\mathcal{L}_{\mathrm{min}} < 0$ outside the contour corresponding to the data is recorded. Since the expected value of the likelihood is positive for all frequencies (see Fig. 3.17b), occasionally the minimum in the range $0 - 19\,\mathrm{ps}^{-1}$ is also positive. These minima are not counted, independently of the frequency at which they occur, since they can not be interpreted as a signal of oscillations.

The population of the toy experiments in the $(\Delta\mathcal{L}, \omega)$ plane along with the point corresponding to the data sample, is shown in Fig. 3.19.

The confidence level is computed as

$$1 - \mathrm{C.L.} \;\equiv\; \frac{N_{\mathrm{exp}}^{\mathrm{out}}}{N_{\mathrm{exp}}} \;=\; 0.021 \pm 0.003\,. \tag{3.38}$$

The study is repeated with 2000 samples of type **S'**, and yields

$$1 - \mathrm{C.L.} \;=\; 0.033 \pm 0.004\,. \tag{3.39}$$

This value has to be understood as a conservative estimate of the probability of statistical fluctuations, since it is obtained with experiments built to have lower point–to–point correlations than that expected for the average of real analyses. The distribution of the minima
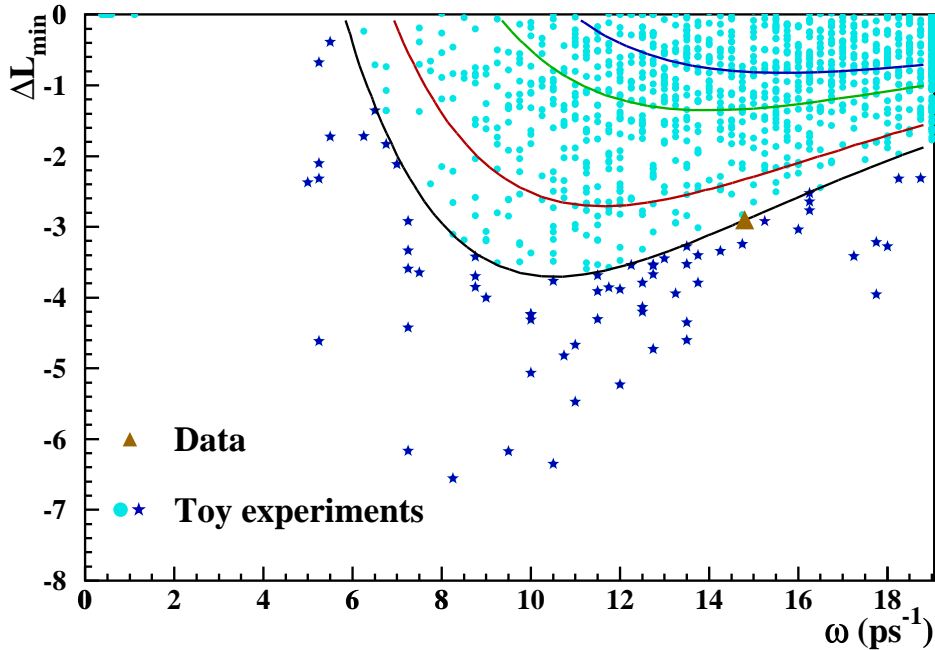
Figure 3.20: Minima of $\Delta\mathcal{L}$ for 2000 samples of type $\mathbf{S'}$ with $\Delta m_\mathrm{s} = 150\,\mathrm{ps}^{-1}$. The same curves as in Fig 3.19 are shown.

for this case is shown in Fig. 3.20. The difference between the values of Eq. 3.38 and Eq. 3.39 gives an upper limit for the uncertainty coming from the lack of a detailed simulation.

The probability that the winter 1999 result of the world combination of B_s oscillation analyses was due to a statistical fluctuation can be therefore quantified to be around 3%. The uncertainty on this number coming from the inaccuracies of the simulation is below 1%.

Comparison with the oscillation hypothesis

In order to check that the amplitude spectrum observed in the data is in qualitative agreement with the hypothesis of oscillations, 500 samples of type $\mathbf{S}$ have been produced, with input frequency $\Delta m_\mathrm{s} = 14.8\,\mathrm{ps}^{-1}$. The expected amplitude and uncertainty at each frequency value are shown in Fig. 3.21, with the data points superimposed. The agreement is good over the whole frequency range.

A quantitative study of the compatibility of the data with the signal hypothesis would require to perform a fine scan on Δm_s with many samples at each value, in order to define a probability that the results observed are produced by an oscillation with a frequency in the range explored. This kind of study is not attempted here.

A simple check is performed instead. The 500 samples with the true oscillation at a value $\Delta m_\mathrm{s} = 14.8\,\mathrm{ps}^{-1}$ are analysed in terms of their incompatibility with the no–oscillation hypothesis. The scatter plot of the likelihood minima in the $(\overline{\Delta\mathcal{L}}, \omega)$ plane, as for the samples with $\Delta m_\mathrm{s} = 150\,\mathrm{ps}^{-1}$, is presented in Fig 3.22.

An enhanced density in the region $14\,\mathrm{ps}^{-1} < \omega < 16\,\mathrm{ps}^{-1}$, $-3 < \Delta\mathcal{L}_\mathrm{min} < -1$ is shown
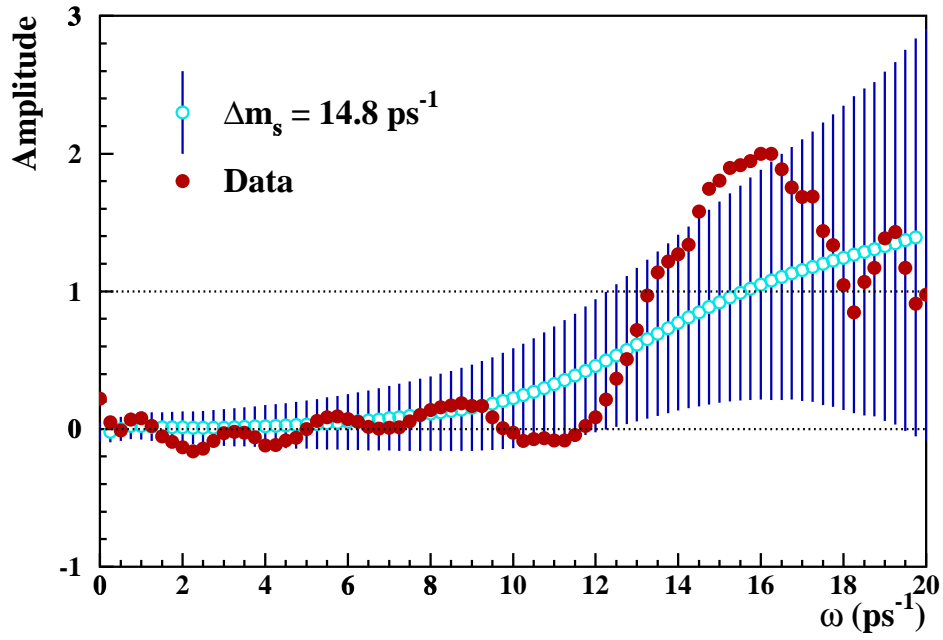
Figure 3.21: Average amplitude and expected uncertainty as a function of ω for a signal at $\Delta m_{\mathrm{s}} = 14.8\,\mathrm{ps}^{-1}$. The amplitude values, obtained by averaging 500 toy experiments, are in good agreement with the data measurements (solid points).

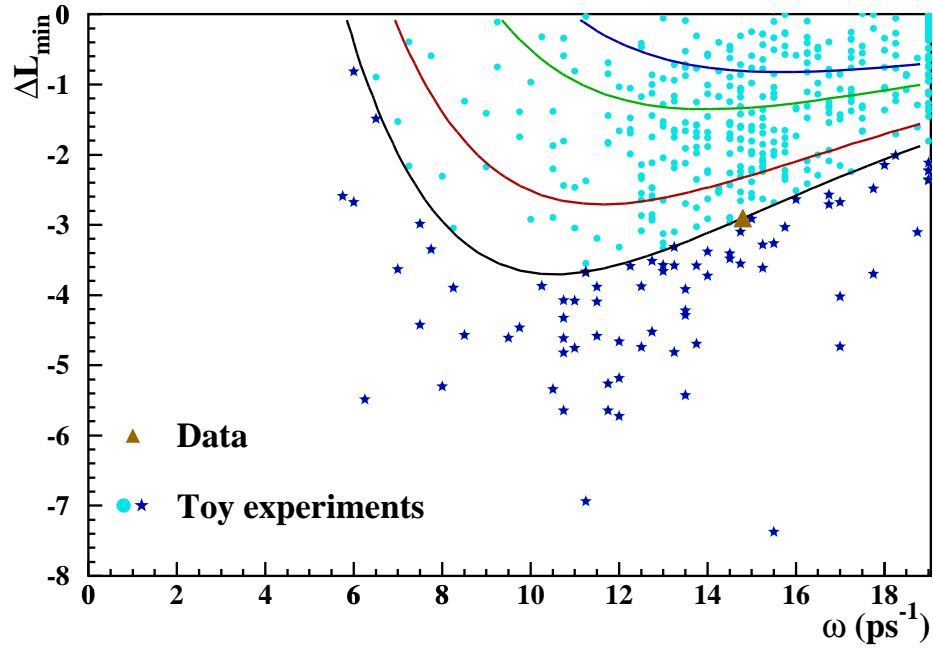Figure 3.22: Minima of $\Delta\mathcal{L}$ for 500 samples of type **S**, with $\Delta m_{\mathrm{s}} = 14.8\,\mathrm{ps}^{-1}$. The same curves as in Fig. 3.19 are shown.

in the plot. A cluster of experiments with minima at $\omega = 19\,\mathrm{ps}^{-1}$ is also clearly visible: for these experiments the lowest point of the likelihood was at the boundary of the region analysed. Experiments with $\Delta\mathcal{L}_{\mathrm{min}} < -5$ appear at frequencies lower than the true one, where fluctuations which can produce deep minima are more likely.

Out of these 500 samples, 80 were found outside the estimator contour corresponding to the data, which gives a probability of 16%. If the data results were perfectly "typical" compared to the toy samples, the expected result would be 50%.

3.3.5   Sensitivity limiting factors

Different factors determine the performance of a $\mathrm{B_s}$ oscillations analysis and its relevance at high values of ω, where the present interest is. Toy experiments are very useful to simulate the impact of each analysis ingredient (such the number of events, the resolution on the momentum or on the decay length) on the final shape of the amplitude statistical uncertainty as a function of the test frequency ω. The toy experiments described in Section 3.3.3 are also used here.

For a $\mathrm{B_s}$ oscillations analysis with N selected events, a $\mathrm{B_s}$ fraction f_{s}, a total mistag probability η_T, and momentum and decay length resolutions σ_p/p and δ_l, the statistical uncertainty on the measured amplitude as a function of the test frequency ω is given by Eq. 3.27. This equation shows that the number of events, the global mistag probability, and the fraction of signal events in the sample contribute to the normalization of the uncertainty distribution without affecting its shape.

Proper time resolution

The proper time resolution affects the shape of the amplitude statistical uncertainty as a function of ω. In general, a better resolution corresponds to a smaller degradation of the precision on the amplitude at high frequency. The two components from which the proper time is estimated have a different impact on the shape of the uncertainty. Toy experiments can be used in this case to illustrate separately the effect of σ_l and σ_p/p. In Fig. 3.23 all uncertainty lines are obtained from the average of 20 samples with $N = 20000$, $f_{\mathrm{s}} = 15\%$, $\eta_T = 25\%$, the resolutions are varied as follows.

  - The reference sample, full line: $\sigma_l = 200\,\mu\mathrm{m}$, $\sigma_p/p = 15\%$.

  - Varying momentum resolution, dash-dotted line: $\sigma_p/p = 7\%$.

  - Varying momentum resolution, dash-dotted line: $\sigma_p/p = 4\%$.

  - Varying decay length resolution, dashed line: $\sigma_l = 160\,\mu\mathrm{m}$.

  - Varying decay length resolution, dashed line: $\sigma_l = 250\,\mu\mathrm{m}$.

For values of the frequency smaller than $\sim 1.5\,\mathrm{ps}^{-1}$, all the curves coincide: the proper time resolution does almost not affect the uncertainty curve in that region. However, as the frequency increases, the effect of varying one of the two resolution components becomes visible. An improvement of the momentum resolution leads to a flatter curve at mid-range
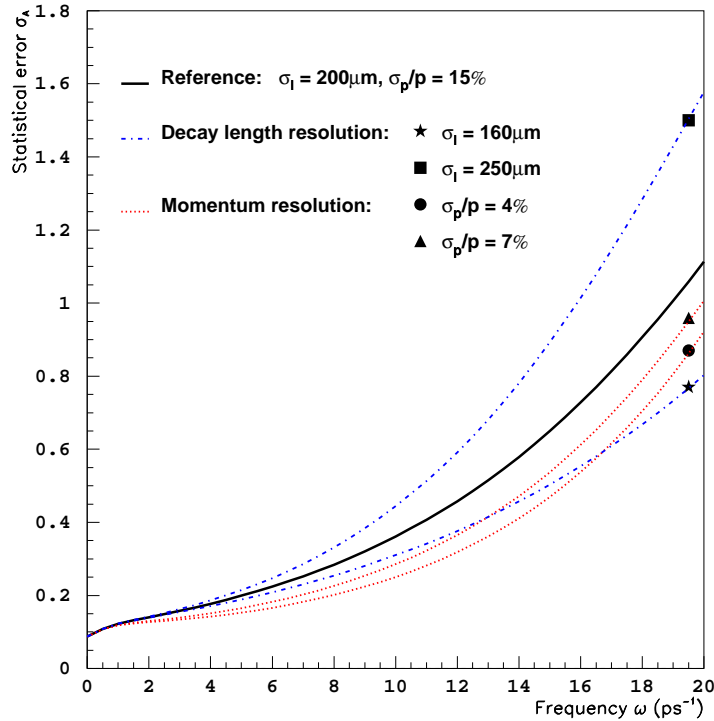
Figure 3.23:   Proper time resolution effect on the amplitude uncertainty. The decay length and momentum resolutions are varied in turn to illustrate their separate impact on the shape of the amplitude uncertainty as a function of ω.

frequencies $\sim 1.5 - 12\,\mathrm{ps}^{-1}$, but the uncertainty curve remains as steep as the reference one, at high frequency. A change of the decay length resolution results in a change of the slope of the uncertainty curve for all values of the frequency ω, this effect is particularly important in the region of interest, at high frequencies. The different impact observed for σ_l and σ_p/p, shows the crucial rôle of the decay length resolution in a B_s oscillation analysis.

Event-by-event decay length uncertainty

In all toy experiments presented up to here, the same decay length resolution is taken for the smearing of all events in the generated sample and this resolution is then used in the fitting function. However, in a real analysis not all events have their secondary vertex re-constructed with the same uncertainty. It is important to use an event-by-event estimate of the uncertainty and not the average of the sample. To illustrate this last point, 20 samples of 20000 events with different decay length resolution values (18% at $80\,\mu$m, 35% at $150\,\mu$m, 27% at $210\,\mu$m, 10% at $350\,\mu$m, 10% at 1.1 mm) were generated. Two different fits were performed; in the first case, each event was fit using the decay length resolution it had been generated with, in the second, all events were fit with the average resolution of the whole sample ($\sim 270\,\mu$m). The other parameters σ_p/p, f_s, and η_T were chosen as in the reference sample used in the previous Section.
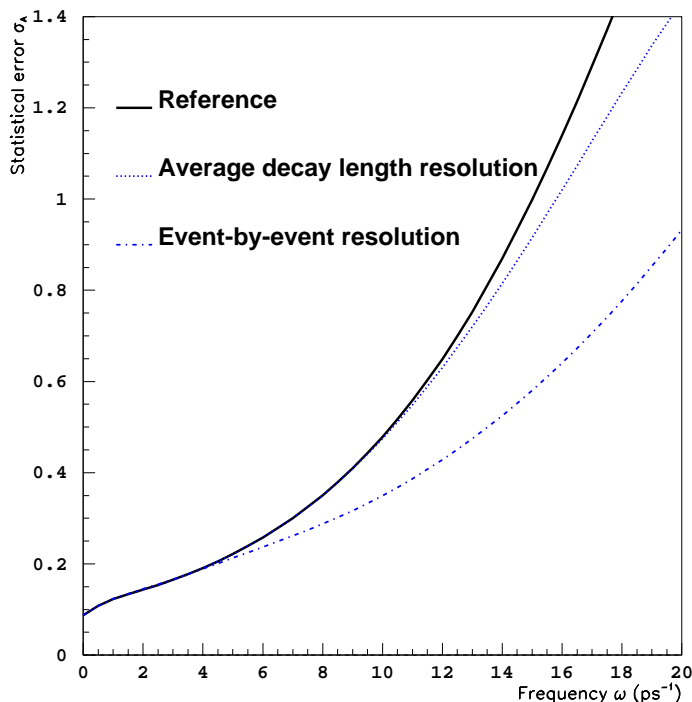
Figure 3.24: Effect of the decay length resolution treatment on the amplitude uncertainty. The use of event-by-event uncertainties is compared to the use of the average uncertainty.

The result is shown in Fig. 3.24. The dash-dotted line corresponds to the fit where each event was treated with its own decay length resolution. The same fitting function was used for the reference line and for the dotted line, with a single resolution value of $270\,\mu$m. The difference between these last two uncertainty curves (full and dotted) is due to the presence of some events with very small decay length resolution in the second sample. The fit is sensitive to these events, even if they are not treated at their best. However, the big difference is appreciated between the dotted and the dash-dotted lines. The event samples are exactly the same: the difference illustrates that an adequate event-by-event characterization increases significantly the potential of a B_s oscillation analysis.

This little exercise shows how much can be gained just by using event-by-event uncertainties, or dividing the sample in resolution classes at least. This point is also illustrated with the real data sample used for the inclusive semileptonic analysis presented in this thesis, in Chapter 8.